MONASH MOTORSPORT

FINAL YEAR THESIS COLLECTION

Design and Development of Carbon Fibre Wheel Shells and Wishbones for a Formula Student Racecar

Daniel Crowe - 2019

The Final Year Thesis is a technical engineering assignment undertaken by students of Monash University. Monash Motorsport team members often choose to conduct this assignment in conjunction with the team.

The theses shared in the Monash Motorsport Final Year Thesis Collection are just some examples of those completed.

These theses have been the cornerstone for much of the team's success. We would like to thank those students that were not only part of the team while at university but also contributed to the team through their Final Year Thesis.

The purpose of the team releasing the Monash Motorsport Final Year Thesis Collection is to share knowledge and foster progress in the Formula Student and Formula-SAE community.

We ask that you please do not contact the authors or supervisors directly, instead for any related questions please email info@monashmotorsport.com

DESIGN AND DEVELOPMENT OF CARBON FIBRE WHEEL SHELLS AND WISHBONES FOR A FORMULA STUDENT RACECAR

DANIEL CROWE

SUPERVISED BY: DR. SCOTT WORDLEY

SUMMARY

This project sets out to design carbon fibre wheel shells and wishbones for the 2019 Monash Motorsport racecars. By utilising composite materials, these structural suspension components can be designed to be lighter, stiffer and more reliable than their aluminium and steel counterparts. This project undertakes advanced composite simulation using ANSYS Composite PrepPost. 3D printed titanium structural members were investigated for use in the carbon fibre wishbone assembly. Carbon fibre wishbone links were mechanically tested to validate the design and manufacturing methods. Overall, the carbon fibre wheel shells saved 3760 g and the carbon fibre wishbones saved 1717 g across each car.

TABLE OF CONTENTS

1. INTRODUCTION

Monash Motorsport is a Formula Student team from Monash University. The Formula Student competition is the world's largest student engineering design competition, where the aim is to design, manufacture, test and compete with an open wheel race car across a series of events. Across the 2018 – 2019 period, Monash Motorsport has competed in the Formula Student UK, Formula Student Austria, Formula Student Germany, Formula SAE Australasia and Formula Student Sydney competitions.

Each competition is comprised of a series of both dynamic (on-track) and static (off-track) events. The results from each event are calculated into points, with a maximum of 1000 points available at competition. A breakdown of the Formula Student Germany events is shown in Table 1. With this knowledge, Monash Motorsport utilizes a simple point-mass simulator to predict the effect that major concept changes, such as mass and power, have on the points scored at competition. The results of this simulation (sim), shown in Figure 1 and Figure 2, were used to drive the early design decisions of the 2019 combustion and electric cars – M19-C and M19-E.

Table 1 At Formula Student Germany the teams compete in 3 Static and 5 Dynamic events, with a maximum of 1000 points available (Formula Student Germany, 2018).

	Discipline	**Points**
Statics	Business Plan	75
	Cost and Manufacturing	100
	Engineering Design	150
Dynamics	Acceleration	75
	Skid Pad	75
	Autocross	100
	Endurance	325
	Efficiency	100
	Overall	**1000**

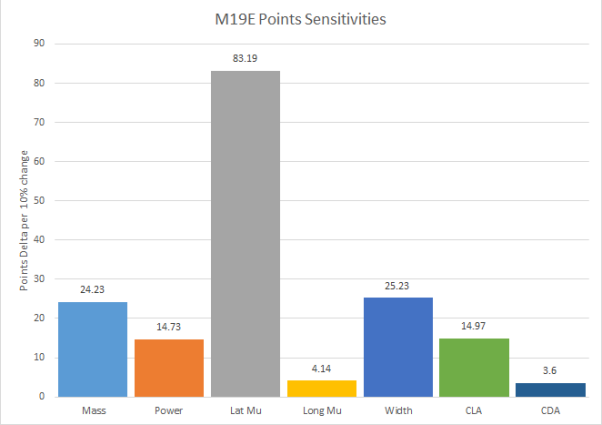

Figure 1 Points sensitivity analysis for M19-E using the simple point-mass sim. The results are displayed as the points gained at competition per 10% parameter change.

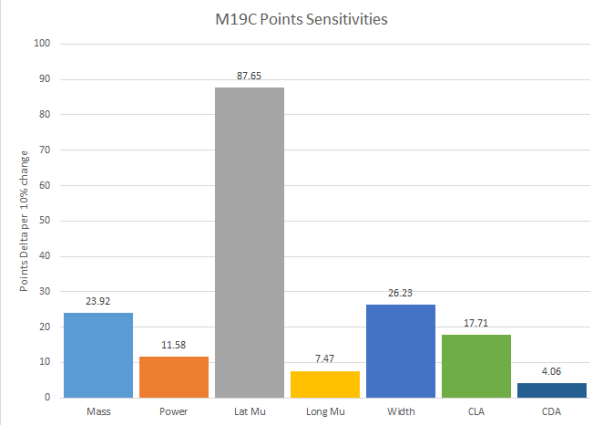

Figure 2 Points sensitivity analysis for M19-C using the simple point-mass sim. The results are displayed as the points gained at competition per 10% parameter change.

Based on the results of extensive tyre testing performed at the end of 2018, Monash Motorsport will move from the 10-inch Hoosier R25b tyres to the 13-inch Goodyear D2704 tyres. Currently, the tyres mount to a three-piece wheel assembly, comprising of two aluminium wheel shells and an aluminium wheel centre that mounts to the hub, shown in Figure 3.

Figure 3 M18-E with a three-piece aluminium wheel supporting the 13-inch Goodyear wet tyre. The same concept will be used in 2019, with the dry Goodyear D2704 tyres and a redesigned wheel centre.

The 2019 suspension geometry is comprised of a double wishbone design, previously manufactured from AISI 4130 alloy steel. By utilizing carbon fibre, these structural suspension components can be designed lighter, stiffer and stronger than previous aluminium and steel designs, increasing the performance of Monash Motorsport's 2019 Formula Student racecars.

The purpose of this project will be to:

- Design carbon fibre wheel shells to mount to the 13-inch Goodyear tyres
- To develop a manufacturing process encompassing mould design, the carbon fibre layup procedure and post-machining methods that can be performed in-house
- Design carbon fibre wishbones utilizing 3D printed titanium bearing cups
- Validate the adhesive bonding by mechanically testing the wishbone links in tension, compression and fatigue.

2. CARBON FIBRE WHEEL SHELLS

In 2014, Monash Motorsport first began a feasibility study into the design of carbon fibre wheel shells (Scott, 2014), with the first carbon fibre wheel shells manufactured in 2015 for 10-inch Hoosier tyres. A similar approach will be taken to design and manufacture the carbon fibre wheel shells for the 13-inch Goodyear tyres.

Figure 4 M18-C with the 10-inch Hoosier tyres and carbon fibre wheel shells, first manufactured in 2015.

2.1 Concept Selection & Benchmarking

Designing carbon fibre wheels allows Monash Motorsport to explore different wheel concepts. Three different concepts utilizing composite manufacturing methods are considered below.

A one-piece wheel – combining the inner shell, outer shell and wheel centre into one component that mounts directly to the hub – would produce the lightest wheel possible (Figure 1). This design would minimise the total parts and fasteners associated with fastening the centre and shells together, saving the mass of an aluminium wheel centre and fasteners. An increase in stiffness could also be expected by designing load paths more directly through carbon fibre without distributing the loads

through fastened joints. This concept is also the most complex to design and time consuming to manufacture, involving multiple complex mould manufacturing and carbon fibre layup processes. A two-piece wheel could join together the inner and outer shells, and bolt directly to the wheel centre (Figure 6). This would save mass by removing some of the fasteners involved in fastening the two wheel shells together, while utilising the existing wheel centres as part of the design. Compared to a three piece design, manufacturing this concept would require additional steps and thus increase the manufacturing time.

Figure 5 A one-piece carbon fibre wheel design by TU Graz Racing Team.

Figure 6 A two-piece wheel design by Revolve NTNU.

A three-piece carbon wheel (Figure 7) will require the same fasteners and wheel centre as the existing three-piece aluminium wheel shell assembly. This minimises opportunities to save mass in areas other than the wheel shells. However, Monash Motorsport currently require the complete disassembly of the wheel shells to change over a set of tyres without damaging the carbon fibre wheel shells, therefore this concept has been selected. Significant mass savings can still be made through the wheel shells whilst increasing stiffness, allowing maximum interchangeability with the aluminium wheel shells and centres, decreasing the design and manufacture time and minimising mould complexity. The three-piece design requires sealing between the inner and outer wheel shells. While a gasket sealant could be used, this would require thorough cleaning every time a new set of tyres is mounted. Therefore, an O-ring seal will be incorporated into the design (Figure 8).

Figure 7 The 2017 Monash Motorsport three-piece wheel design, featuring carbon fibre wheel shells and an aluminium wheel centre.

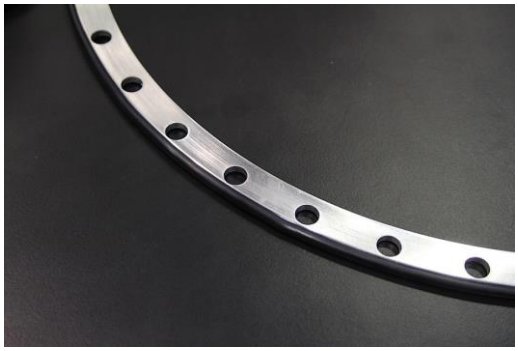

Figure 8 A nitrile O-ring, seated by an aluminium spacer, can form a seal between the two wheel shells.

Monash Motorsport currently has a stock of sponsored Pre-impregnated Carbon Fibre (Pre-Preg). This prepreg is a high temperature cure (177^{o}C), and its material properties have been validated through strain gauge mechanical testing (McRedie, 2015). The material properties are described in more detail in the advanced analysis section of this report (Section 3.0). The prepreg carbon fibre provides adequate draping for the geometry of the wheel shells, so this carbon fibre will be used for the wheel shell design and manufacture.

In 2015, Monash Motorsport first designed and manufactured carbon wheel shells for use with the 10-inch Hoosier tyres shown in Figure 4. These shells gave a 31% mass reduction (1253 g per wheel) compared to the previous aluminium shells (1822 g per wheel). The current aluminium wheel shells for the 13-inch Goodyear tyres are 2007 g per wheel. Assuming a similar mass reduction, Monash Motorsport stands to lose 622 g per wheel, totaling 2488 g across each car.

2.2 Justification & Points Analysis

The carbon fibre wheel shells are expected to improve performance by decreasing mass and increasing stiffness. From the simple sim results in Figures 1 and 2, the mass targets correspond to 2.7 points gained at the competition for M19-E and 3.3 points gained for M19-C. Camber compliance sensitivities for the new Goodyear tyres are under investigation with the advanced vehicle model simulator, however these sensitivities were unknown at the time of this report, so no target was set. Camber compliance was still measured during the advanced analysis to determine the increase in performance when these sensitivities are determined.

2.3 Rim Width & Offset Selection

The Goodyear D2704 13-inch tyres are designed for a 7-inch rim width. It is possible to stretch the tyres onto a 7.5-inch or even 8-inch rim, which could increase the cornering stiffness of the tyre at the expense of maximum lateral coefficient of friction. In 2015, Monash Motorsport found that stretching the 7.5-inch wide Hoosier tyres onto 8-inch rims increased the response of the tyres, with an increase in cornering stiffness allowing the tyres to reach peak lateral acceleration faster, therefore spending more time at higher lateral acceleration compared to the unstretched tyres. It was decided not to repeat this testing at this stage of the 2019 design and manufacture timeline. Testing tyre parameters is resource intensive, both in terms of the price of a set of tyres and the man-hours involved in a testing session. Testing toe, camber and tyre pressure parameters on the 7-inch rims were given priority to find an initial best setup for the new tyres. This testing will occur at the start of the 2019 testing period scheduled after the Monash University first semester exam period. Rim width testing may occur after testing these other parameters if resources allow. In comparison to the Hoosier R25b tyres, the Goodyear tyres have a much higher cornering stiffness (as seen from TTC data), and this may be seen as a parameter that does not justify resource-intensive testing. In addition, no tyre testing data is available from the TTC with the tyres mounted to 8-inch rims, as these tyres experienced de-beading during the test warmup procedure. This raises concerns over the safety and reliability of stretching the Goodyear tyres on the M19 racecars. For these reasons, a 7-inch rim design was selected.

Wheel offset is defined as the distance between the centreline of the wheel to the hub mounting point (Figure 9). Wheel offset affects the ability to package the outboard assembly within the wheel to decrease the scrub radius, which is related to steering effort. Steering effort was raised as a concern by drivers during the Goodyear tyre testing session, so the front offset was designed as

large as possible to decrease the scrub radius. The minimum aluminium outer shell thickness available was 1.5-inch, and when paired with a 5.5-inch inner shell, the front offset came to 2-inch. With a custom mould for the carbon fibre shells, a 2.5-inch offset with a 1-inch outer shell and a 6-inch inner shell could be achieved. However, for maximum compatibility between the aluminium and carbon fibre shells, it was decided to design and manufacture the shells to have the same 2-inch offset at the front, and zero offset at the rear.

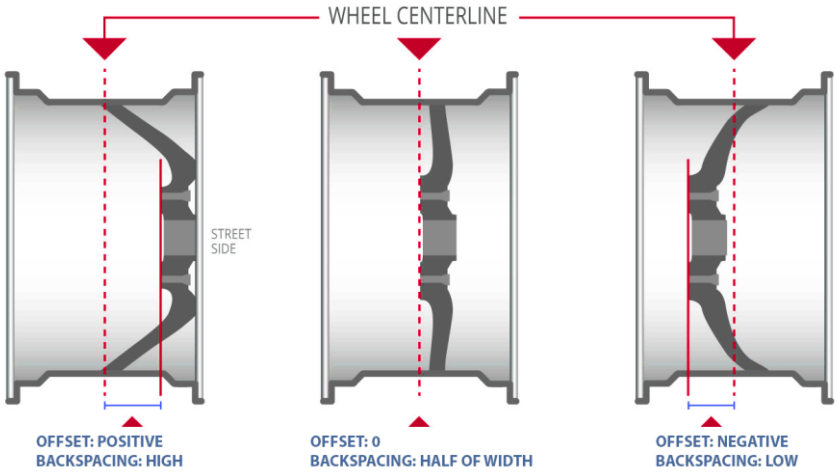

Figure 9 Wheel offsets diagram. The M19 racecars will feature a positive offset at the front and no offset at the rear (Element Custom Wheels and Tires, 2019).

3. ADVANCED ANALYSIS

Monash Motorsport currently has access to ANSYS 19.2 ACP simulation software. This will be used for the advanced analysis of the wheel shells. Accurate simulation results require a detailed understanding of the boundary conditions, and how these can be closely modelled with the software. The current ANSYS three-piece wheel model, used for wheel shell and wheel centre analysis by Monash Motorsport, is outlined below, with detailed images attached in the appendix.

ACP allows for composite laminated to be accurately modelled by assigning global fibre orientations (Figure 52) and applying known orthotropic material properties (Figure 10). This allows carbon fibre layer stacks and orientations to be designed effectively to reduce mass, increase stiffness and maximise reliability. The ACP-Post module provides several failure criteria tools to be applied to the analysis, depending on the stresses being investigated (ANSYS, 2017). These failure criteria will be further investigated and compared in the report.

3.1 Simulation Setup

The prepreg is a 3K tow weave with a mass of 193 g/m^2 and 50% resin mass. Its material properties were measured by strain-gauges by McRedie, 2015, and its properties were found to most closely align with the Epoxy Carbon Woven (230 GPa) Prepreg composite material in ANSYS.

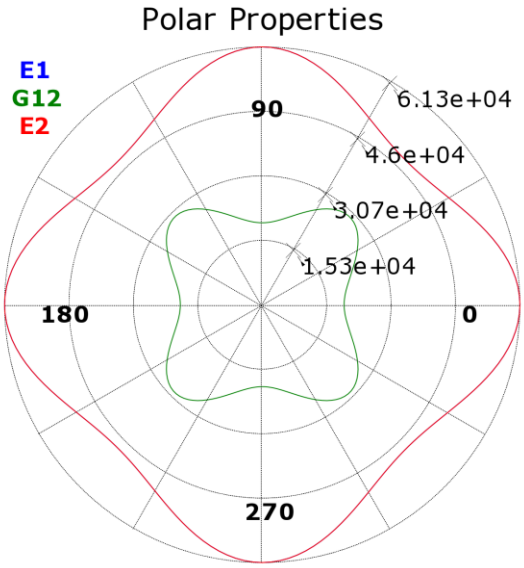

Figure 10 Polar properties of the Epoxy Carbon Woven (230) GPa) Prepreg composite material in ANSYS, visualizing the difference in properties between a 0^o and 45^o ply orientation.

There are four components: the inner and outer wheel shells, the wheel centre and a spacer that seats the O-ring (Figure 11). The wheel shells are imported as faces from which thickness is built up as carbon fibre plies are added. Frictional contacts are used at all contact surfaces: between the inner and outer wheel shells to the spacer (Figure 12) and the outer wheel shell to the wheel centre. A fixed support is added to the wheel centre where it would contact the hub.

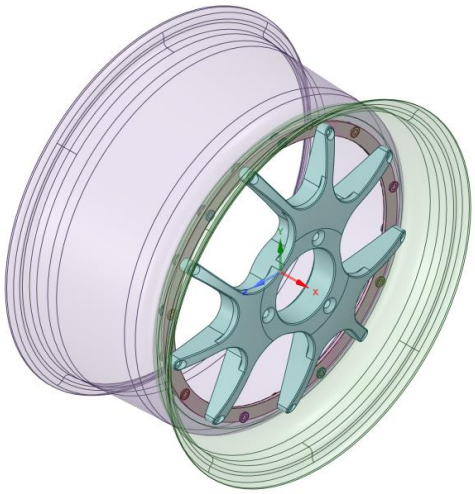

Figure 11 The FEA model for wheel shell structural analysis, featuring a solid body wheel centre and spacer, and wheel shell faces before adding thickness through ACP carbon fibre stack-ups.

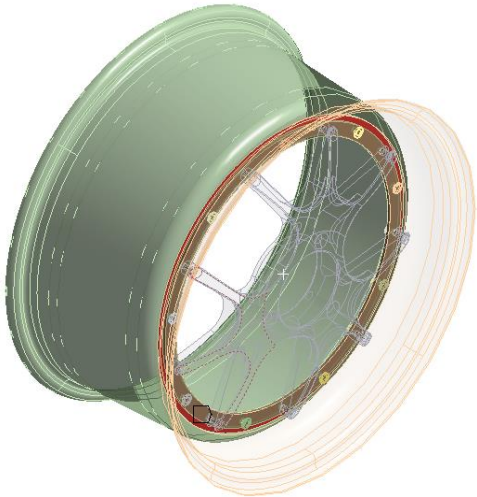

Figure 12 A frictional contact is applied between the inner wheel shell face and the spacer.

Washer faces are added to each of the bolt holes. Spring joints with a preload are added to represent the bolts, connecting to either the washer faces on the inner to the outer shell, or the inner shell to the wheel centre (Figure 46).

The shell faces were split into segments to be able to increase the carbon fibre thickness where necessary, but to minimise mass where thickness was not necessary (Figure 13).

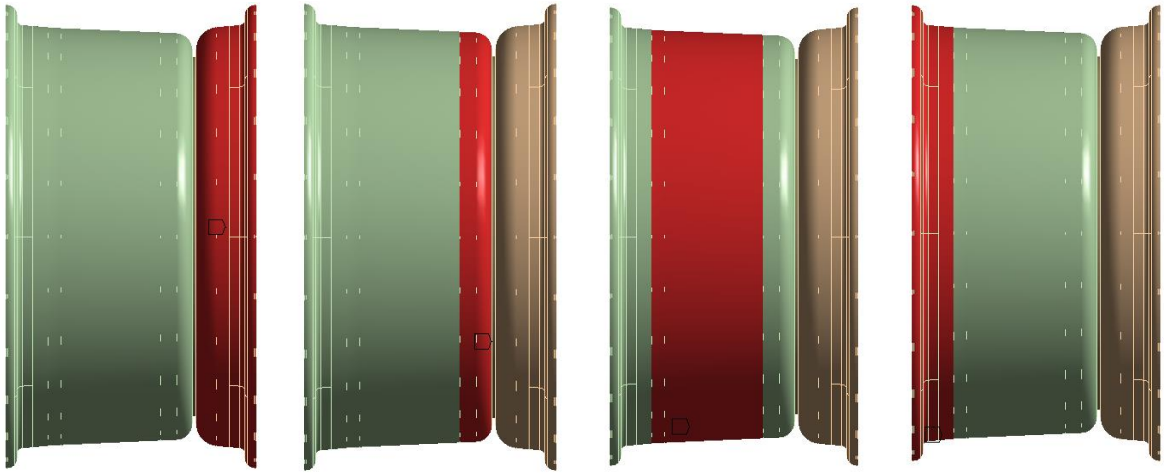

Figure 13 The wheel shells are divided into segments, from 1 (left) to 4 (right).

Using the Epoxy Carbon Woven (230 GPa) Prepreg material, the thickness is defined in fabric properties to 0.22 mm to give the prepreg a single ply thickness (Figure 47). Stack-ups are created by defining the number and orientation of plies, as well as the direction of the carbon fibre stack-up and stack-up symmetry (Figure 48).

A rosette is used to define a reference orientation at each element for the carbon fibre directions. Using an edgewise rosette in ACP, the profile of the wheel shells can be followed. Two reference directions are given, for the 0^o and 90^o carbon fibre ply orientations (Figure 49).

The rosette is then mapped to each segment, to give the elements within each segment their reference carbon fibre directions. With the oriented element sets complete, the selected carbon fibre stack-ups are applied to each segment (Figure 50).

The contact patch forces are applied as a remote force originating from the contact patch (Figure 53). The forces act through the tyre beading surfaces. Due to the complex nature of tyre physics, the load transfer between the tyre and the wheel shells is difficult to calculate. The distribution of forces through the bead are approximated and detailed in Figures 55-60.

Contact patch forces are calculated using the suspension geometry of the car and the predicted maximum load cases in a number of directions.

Table 2 Vehicle load cases and front wheel contact patch forces used for simulation inputs.

Front wheel load case	Longitudinal acceleration	Lateral acceleration	Contact patch Fx	Contact patch Fy	Contact patch Fz
Pure lateral	0 g	-2.4 g	0 N	-2909 N	2060 N
Combined 1	-1.55 g	-1.55 g	-2022 N	-2022 N	2217 N
Braking	-2 g	0 g	-2153 N	0 N	1829 N
Bump	-1.55 g	-1.55 g	-2022 N	-2022 N	8958 N
Inside wheel	0	1.8 g	0 N	702 N	633 N

Table 3 Vehicle load cases and rear wheel contact patch forces used for simulation inputs

Rear wheel load case	Longitudinal acceleration	Lateral acceleration	Contact patch Fx	Contact patch Fy	Contact patch Fz
Pure lateral	0 g	-2.4 g	0 N	-3227 N	2285 N
Combined 3	0.8 g	-1.5 g	1734 N	-1899 N	2151 N
Acceleration	1.2 g	0 g	1825 N	0 N	1663 N
Bump	-1.55 g	-1.55 g	-1372 N	-1372 N	5392 N
Inside wheel	0 g	1.8 g	0 N	636 N	600 N

3.2 Simulation Results

The simulation provided stress and deformation results. These are documented in Tables 4 & 5. The camber compliance was calculated to be 0.16 ^{o}/g at the front and 0.20 ^{o}/g at the rear at the maximum pure lateral load case.

3.3 Composite Failure Criteria

The ANSYS ACP Failure Criteria tool contains several composite failure criteria to analyse the simulation results with. The failure criteria selected for analysis were Tsai-Wu and Tsai-Hill (Kaw, 2006).

The results were given as a safety factor for all failure modes and plies at each node (Figure 14). The results were analysed by segment and by ply throughout the design process, removing or increasing plies where necessary to decrease mass or increase the safety factor respectively. The results are detailed in Tables 4 & 5.

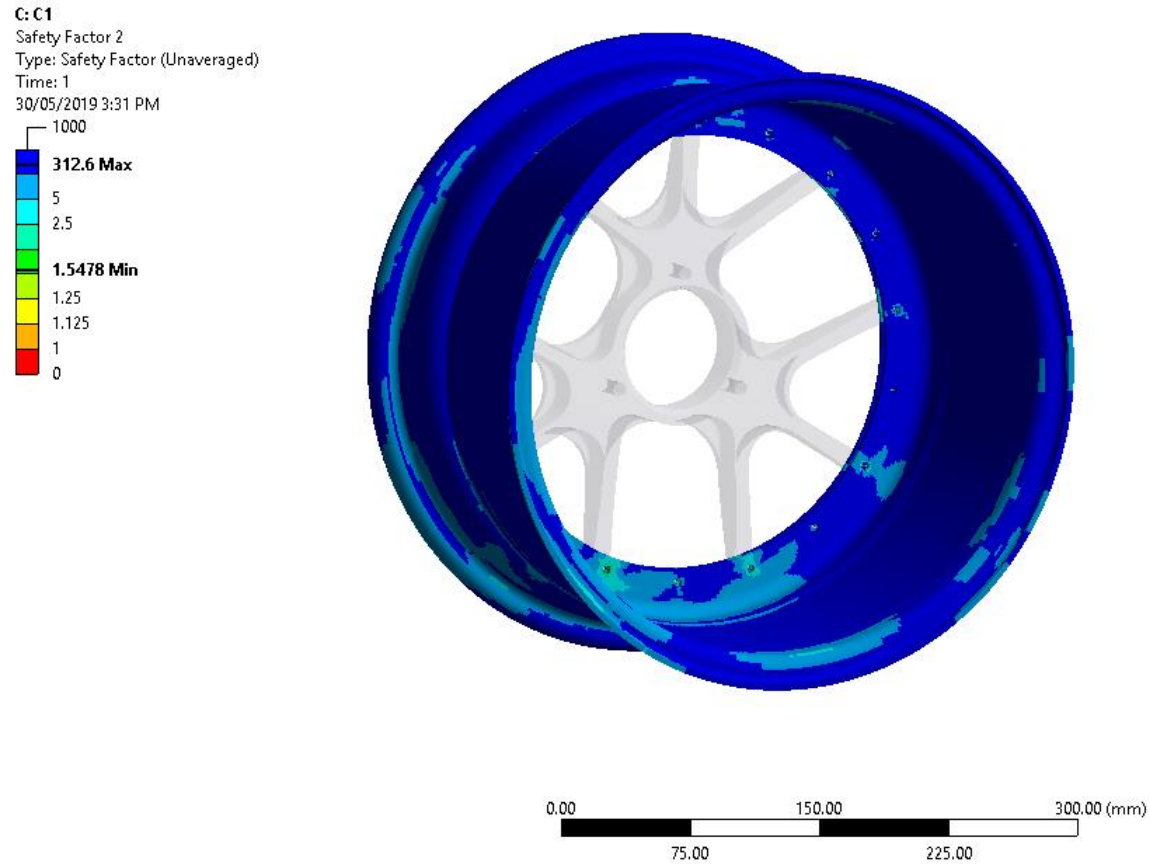

Figure 14 Tsai-Wu and Tsai-Hill minimum safety factor at the front wheel after simulating the combined 1 load case.

Table 4 Simulation results for the front wheel shells for each load case input.

Load case	Max stress (von Mises)	Min safety factor inner shell	Min safety factor outer shell	Max y deformation	Max z deformation	Camber compliance
Pure lateral	229 MPa	1.47	2.02	1.49 mm	1.31 mm	0.32°
Combined 1	232 MPa	1.55	1.71	1.08 mm	1.05 mm	0.07°
Braking	72 MPa	5.29	4.35	-0.23 mm	0.50 mm	-0.16°

Table 5 Simulation results for the rear wheel shells for each load case input.

Load case	Max stress (von Mises)	Min safety factor inner shell	Min safety factor outer shell	Max y deformation	Max z deformation	Camber compliance
Pure lateral	291 MPa	1.14	1.78	1.74 mm	1.30 mm	0.39°
Combined 3	231 MPa	1.43	2.11	0.95 mm	0.72 mm	0.22°
Acceleration	133 MPa	2.90	2.27	0.29 mm	0.26 mm	0.01°

4. FINAL DESIGN

A final carbon fibre ply thickness and mass breakdown is given in Table 7. The result is a 3.76 kg mass saving across each car, resulting in 3.0 points gained at the competition for M19-E and 3.8 points gained for M19-C. The camber compliance results are 0.16 °/g for the front and 0.20 °/g at the rear. These can be used to determine an additional points gain compared to aluminium wheel shells when camber compliance sensitivities are determined.

Table 6 The final design number of plies, thickness and mass of the front wheel shell components.

Front wheel		Ply number	Thickness (mm)	Mass (g)
Outer shell	Segment 1	10	2.20	262
Inner shell	Segment 2	16	3.52	230
	Segment 3	10	2.20	272
	Segment 4	16	3.52	226
O-ring spacer				88
Total				1078

Table 7 The final design number of plies, thickness and mass of the rear wheel shell components.

Rear wheel		Ply number	Thickness (mm)	Mass (g)
Outer shell	Segment 5	12	2.64	162
	Segment 6	10	2.20	136
	Segment 7	12	2.64	163
Inner shell	Segment 8	14	3.08	189
	Segment 9	10	2.20	136
	Segment 10	14	3.08	190
O-ring spacer				88
Total				1062

The wheel shell profile is designed to the JA rim contour (Figure 65) featuring a 5° draft. This draft angle complemented the mould draft angle nicely to allow for the carbon fibre de-moulding.

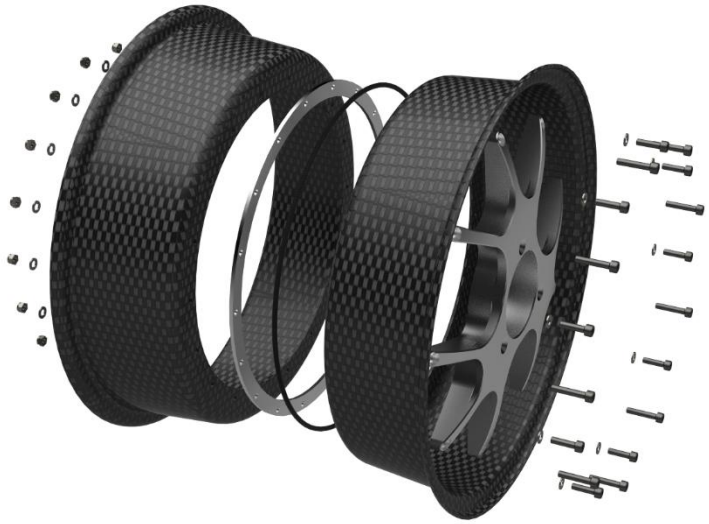

Figure 15 An exploded CAD assembly render of a rear wheel, featuring the wheel shells, centre, O-ring, spacer and fasteners.

4.1 Mould Selection & Design

Scott, 2014 compared the manufacturing results from a male and female mould for carbon fibre wheel shells. It was found that pre-preg carbon fibre layups were more successful using a male mould for the wheel shell geometry.

Mould design will follow a proven method of stacking lasercut steel plates (Figures 16-19), with the aim to reduce as much mass as practical to improve the ergonomics of handling the moulds. An alternative method is to machine a mould from a billet of aluminium, however due to the size of the wheel shells, this is a more expensive method.

The lasercut layers of the mould can be fastened together, and then require machining on a CNC lathe to achieve the wheel shell profile. Three moulds will be required in total – the rear inner and outer shells have the same profile.

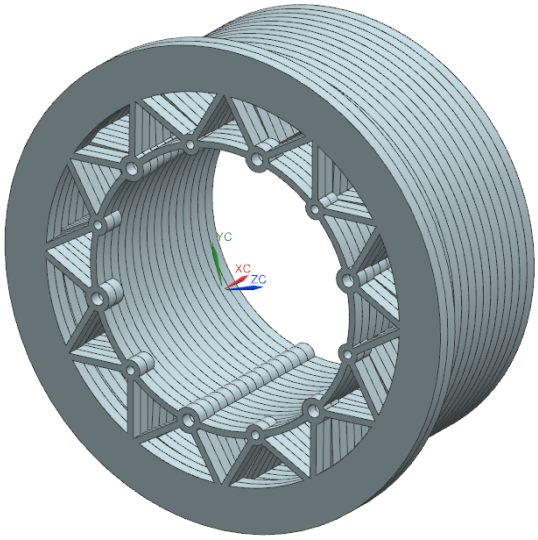

Figure 16 A stack of lasercut steel plates to be bolted together, prior to machining the wheel shell profile.

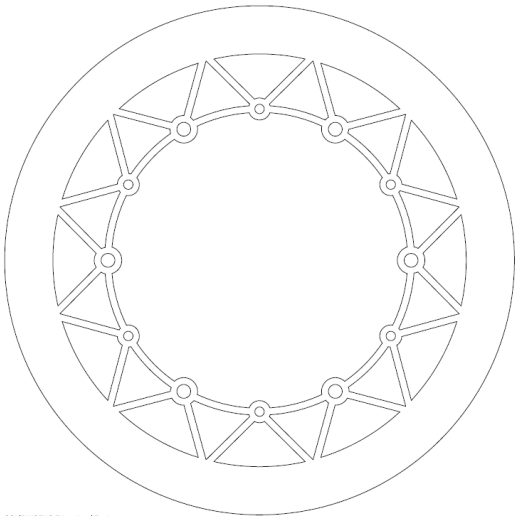

Figure 17 The individual mould layer profile, featuring outer material to be machined down, holes to clamp the mould together, and mass saving where possible to improve the mould ergonomics.

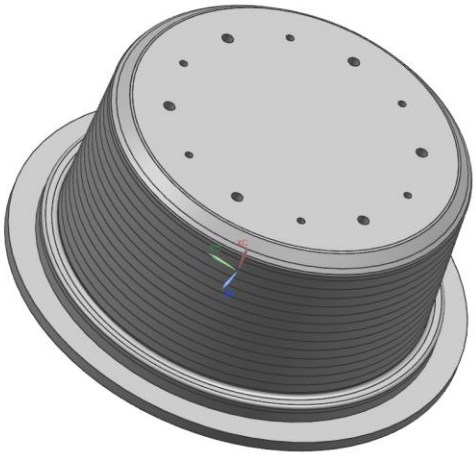

Figure 18 The final mould post-machining top view.

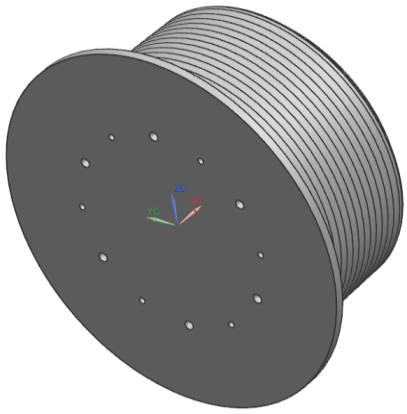

Figure 19 The final mould post-machining bottom view.

4.2 Layup Sequence

To replicate the carbon fibre stack-ups modelled in ANSYS, the layup sequence and orientation of carbon fibre plies was determined through trial and error using an old aluminium wheel shell as a dummy mould. Each wheel shell has its own layup sequence detailed in Tables 22-25.

4.3 Post-Machining

A bolt-on plate at the top of the mould can be used to locate and centre drill the wheel shell holes before the shell is de-moulded. This will allow the holes to be located in the same location every time, without the need to setup a post-machining process. Using these holes, the inside and outside diameters can be ground down using a fixed die grinder with a cutting disk, with the shell bolted to a

jig and rotated concentrically around an indexing head on the mill. This allows all the post-machining to be performed in-house.

5. CARBON FIBRE WISHBONES & LINKS

As in previous years, the Monash Motorsport M19 racecars feature a double wishbone suspension system (Figure 20). The objective of the wishbones is to transfer the tyre contact forces from the unsprung system to the sprung chassis while facilitating the kinematic movements of the wheels through roll, pitch, heave and warp.

Figure 20 The rear right steel wishbones on M17-C.

The maximum forces expected to act through each wishbone and toe link are determined by resolving the contact patch forces through the suspension geometry points. The contact patch forces and resulting wishbone forces are calculated from the load cases in Tables 2 & 3, covering longitudinal acceleration, lateral acceleration and combined acceleration load cases, to give the forces through each wishbone link at each load case. The maximum compression and tension loads through each link are summarised in Tables 8 & 9.

Table 8 Maximum forces acting through the front suspension members.

Front wishbones	Upper fore	Upper aft	Lower fore	Lower aft	Shock	Toe link
Max tension (N)	1868	3470	7474	2313	0	352
Max compression (N)	-2828	-957	-3014	-8043	-1817	-103

Table 9 Maximum forces acting through the rear suspension members.

Rear wishbones	Upper fore	Upper aft	Lower fore	Lower aft	Shock	Toe link
Max tension (N)	988	2730	5820	3083	0	2363
Max compression (N)	-2462	-1910	-2951	-3752	-2057	-1928

5.1 Concept Selection & Benchmarking

Several concepts were investigated for the carbon fibre wishbone design. It is possible to layup custom carbon fibre tubing (Figures 21 & 22), however off-the-shelf carbon fibre tubing was chosen to reduce design and manufacturing complexity.

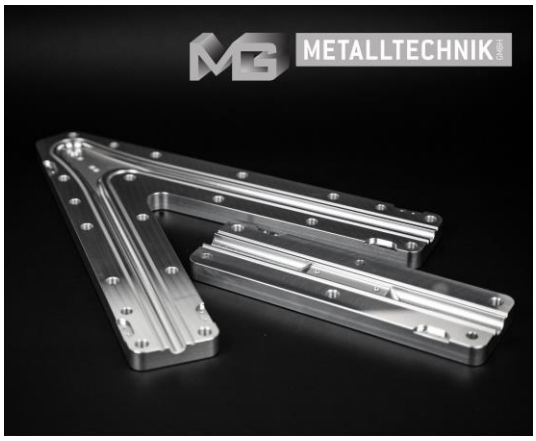

Figure 21 Machined aluminium female moulds for a carbon fibre wishbone layup by TU Wien Racing.

Figure 22 Custom carbon fibre wishbone layup incorporating a machined aluminium bearing cup by TU Wien Racing.

The carbon fibre tubes need to be bonded to a joint at both inboard suspension points to the chassis and at the outboard suspension point to the upright. The inboard joints can be either spherical bearings housed in a bearing cup or threaded rodends. The steel wishbones designed for the Monash Motorsport 2019 racecars feature rodends to allow for suspension geometry adjustment if required. While the rodends are heavier than a spherical bearing, they were chosen for the carbon fibre wishbones for maximum interchangeability with the steel wishbones. In 2018, all the wishbone rodends were PRM-5T Aurora Bearings rodends. These were the smallest rodends in the high-performance range that exceed our required misalignment angle. AM-4T rodends were successfully utilised on our toe links front and rear, and are a smaller and lighter design that meet the design requirements. This year, the wishbone design has saved 180 g per car and $546.00 in total by utilising the AM-4T rodends for all of the upper wishbones (Table 10).

Table 10 Aurora bearing selections for the M19 racecars.

	Type	QTY	Price	Total	Mass	Misalignment	Radial capacity	Radial safety factor
Lower wishbones	PRM-5T	16	$36.25	$580.00	36 g	14°	37054 N	4.6
Upper wishbones & toe links	AM-4T	32	$13.50	$432.00	21 g	16°	23397 N	6.7
Outboards	PWB-5T	16	$20.60	$329.60	18 g	14°	41813 N	7.2

The inboard rodends and outboard spherical bearing both require bonding to the carbon fibre tube. Two bonding concepts were considered: inserts bonding inside the tube or outserts bonding outside the tube. Inserts were chosen due to the higher tolerance on the internal diameter of the carbon tube (±0.15 mm internal tolerance vs ±0.3 mm external tolerance) and the ease of manufacturing an external tolerance on the inserts.

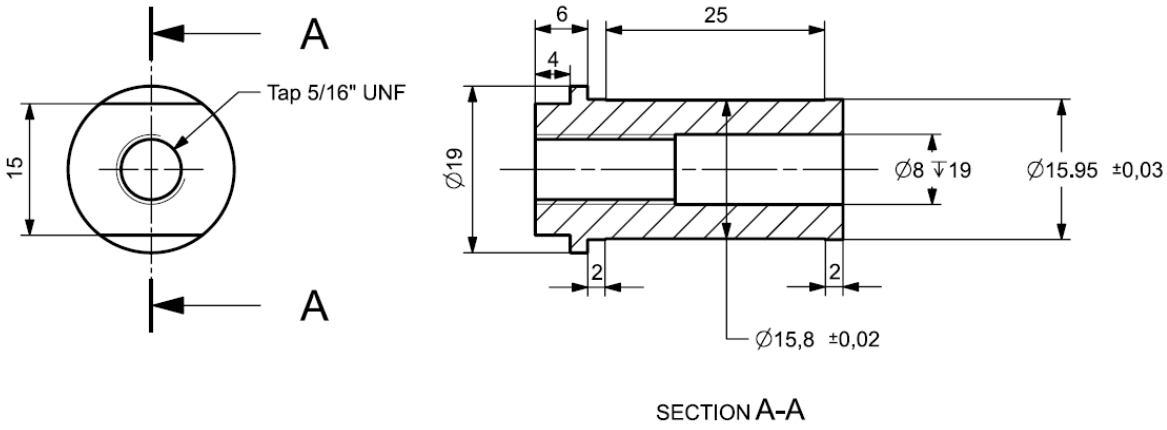

Figure 23 An aluminium insert manufacturing drawing featuring the dimensions and tolerance for the final insert design. Dimensions in mm.

There were two concepts available to consider for the outboard bearing cup design. The first was to CNC the outboard from aluminium billet through existing CNC sponsors. The second was to 3D print the outboard with a new sponsor. Due to the complex geometry and high quantity of parts required, it was decided to pursue a 3D printed concept. Monash Motorsport is grateful to have both CSIRO'S Lab 22 and the Monash Centre for Additive Manufacturing (MCAM) onboard for sponsorship of 3D printed titanium components in 2019.

Figure 24 Machined aluminium inserts and bearing cups by NTNU Revolve.

Figure 25 A 3D printed titanium bearing cup by InMotion (Eindhoven) for an electric racecar.

The steel wishbones in 2018 weighed a total of 4.35 kg. A conservative mass target of 3.5 kg was assigned to the carbon wishbones in 2019.

5.2 Justification & Points Analysis

It was decided to design and manufacture both steel wishbones and carbon fibre wishbones in parallel, with the aim of ensuring that steel wishbones are ready for the chassis rolling deadline of May 30, while the necessary carbon fibre wishbone testing and validation takes place before a final carbon fibre wishbone design can be implemented later in the year. The primary reason behind the move towards carbon fibre wishbones is to save mass by utilising the significantly higher specific strength properties of carbon fibre compared to AISI 4130 steel. A conservative 3.5 kg concept would achieve a 0.9 points gain at the competition for M19-E and a 1.3 points gain for M19-C. It is expected that carbon fibre wishbones can also be made stiffer, however camber and toe compliance sensitivities are currently unknown with the move to the Goodyear tyres. With the mechanical testing and validation to occur this year, it is expected that future designs can be manufactured in a shorter time period than the current steel wishbone design and manufacture, allowing the team to allocate resources elsewhere during the critical manufacturing period.

6. MECHANICAL TESTING

Mechanical testing was performed using the Instron universal testing machine at the Monash Institute of Railway Technology (Figure 26) to validate the strength and fatigue life of the carbon fibre wishbone links. Tension and compression testing occurred at 5 mm/min. Fatigue testing occurred at 1 Hz. All carbon fibre tubes were 100 mm in length, until a final buckling test was performed on a full length 390 mm link. The results are described below.

Figure 26 Buckling test performed on the Instron at 5 mm/min compression.

6.1 Adhesive Testing & Results

Mechanical testing was first used to determine the strongest adhesive and glue gap. Adhesive products from Loctite and 3M were considered. After researching the product range available in Australia, Loctite EA E20HP and 3M DP 490 were chosen for physical testing based on their shear strength specifications when bonded to aluminium and CFRP. A comparison of their key features is shown in Table 11. Glue gaps of 0.1 mm and 0.2 mm were tested, both within the recommended range for both the Loctite and 3M products.

Table 11 Adhesive specification comparison between the selected Loctite and 3M adhesives.

	Loctite E20HP	**3M DP490**
Cure time	24 hours	7 days
Cost per 50 mL	$46.00	$71.00
Aluminium (abraded) bond shear strength	28.2 MPa	23.7 MPa
Aluminium (anodized) bond shear strength	17.4 MPa	
Epoxy shear strength	28.6 MPa	36.1 MPa
Steel (grit-blasted) shear strength	22.6 MPa	
Stainless steel shear strength	22.0 MPa	

The aluminium insert dimensions are shown in Figure 23. The two insert shoulders are designed for a high tolerance sliding fit into the tube to locate the insert concentrically and maintain an even glue gap over the entire surface. The middle section of the insert is dimensioned to provide the appropriate glue gap, with the diameter and length providing the adhesive surface area.

Based on a 20 mm insert length and a conservative adhesive shear strength of 16 MPa (approximately 60% of manufacturer specifications), 16 mm ID carbon fibre tube was selected for testing with the aim of withstanding a minimum of 16 kN in tension. The results are shown in Figures 27 & 28.

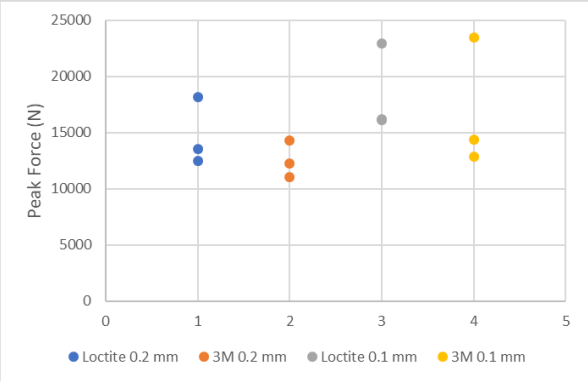

Figure 27 Tension testing results comparing adhesive and glue gap: all aluminium inserts 20 mm in length, roll wrapped tube.

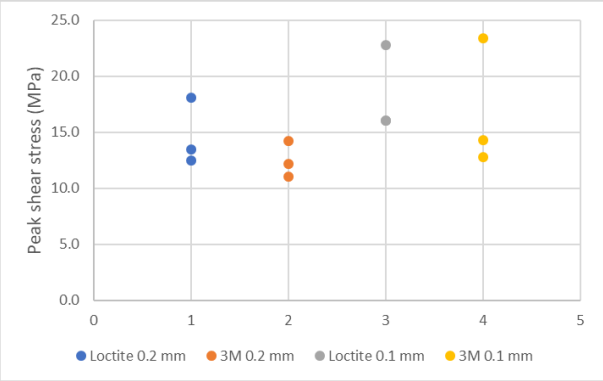

Figure 28 Tension testing results normalised for adhesive surface area: all aluminium inserts 20 mm in length, roll wrapped tube.

The most common failure mechanism was delamination of the inside ply, which indicated that the carbon fibre tube was often the limiting factor. However, failures did also occur at the interface between the adhesive and the aluminium. In general, it can be seen in Figures 27 & 28 that the Loctite out-performed the 3M adhesive when comparing the same glue gap, and the 0.1 mm glue gap out-performed the 0.2 mm glue gap when comparing the same adhesive. The Loctite 0.1 mm glue gap samples were the only samples not to have a failure below 16 kN. While this data was limited in sample size and included failures where the adhesive was not the limiting factor, when combined with the price and cure time differences (Table 11), Loctite E20HP with a 0.1 mm glue gap was selected as the adhesive of choice.

A selection of other carbon fibre tubes were tested to obtain data for more variables. These tests differed in tube composition, tube ID and insert length. The results are shown in Figure 73. When results were normalised for adhesive cross-sectional area, the carbon fibre tube composition proves to be an extremely sensitive parameter. The most common failure mechanism was delamination of the inside tube ply, and this occurred at much higher loading for longitudinally orientated fibres (e.g. pultruded tube) than for tangentially orientated fibres (e.g. the inside layer of the roll-wrapped tube).

6.2 Tube Size Testing & Results

Based on the initial adhesive selection testing, insert and tube sizing was calculated for the final design. 16 mm ID tube was selected for the lower wishbones, with 12 mm tube selected for the upper wishbones and toe links. Filament wound tube was purchased from CST Composites. The filament winding process wraps fibres at 45^{o} to the longitudinal axis. This gives the inner plies of

carbon that bond to the adhesive more longitudinal strength, and higher strength was expected in tension to avoid early carbon delamination failures. The minimum tube wall thickness available at the time was 2 mm, however the supplier can manufacture 1.5 mm wall thicknesses. Insert length was extended to 25 mm to increase the bond strength at a negligible mass increase. Aluminium inserts manufactured in-house and titanium inserts printed by Lab 22 (CSIRO) were both tested. Tension, compression, fatigue and buckling tests were performed to validate the final designs. The results are outlined below in Figures 29 & 30.

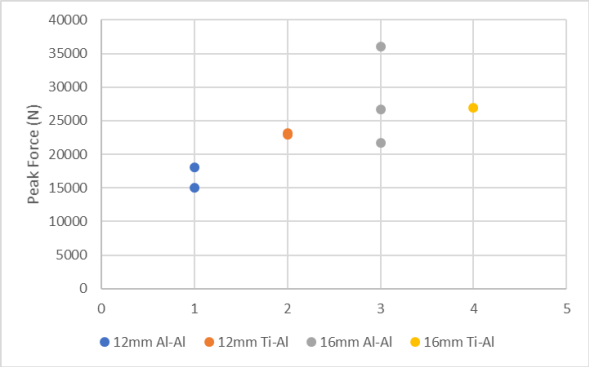

Figure 29 Tension testing results: aluminium and titanium inserts, all 25 mm in length, 0.1 mm glue gap, filament wound tube.

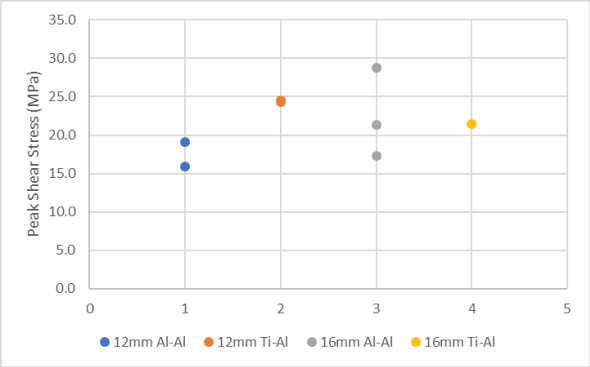

Figure 30 Tension testing results normalised for adhesive surface area: aluminium and titanium inserts, all 25 mm in length, 0.1 mm glue gap, filament wound tube.

Two 12 mm ID tubes with aluminium inserts at both ends failed at 15.0 and 18.0 kN (15.9 and 19.1 MPa respectively). Two 12 mm ID tubes with one aluminium insert and one titanium insert at each end failed at 22.9 and 23.1 kN (24.3 and 24.5 MPa respectively). All 12 mm ID tube failures were due to carbon delamination (Figure 31). With the maximum load case for the 12 mm ID links being 3.47 kN in tension, the testing results gave a minimum safety factor of 4.3.

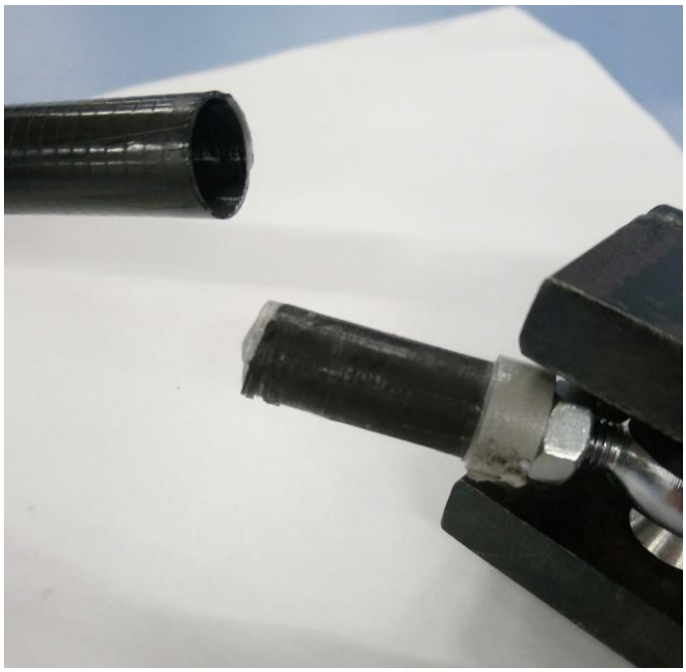

Figure 31 Carbon fibre delamination failure at the inner ply. 12 mm ID filament wound tube, 25 mm length aluminium insert, 0.1 mm glue gap.

Three 16 mm ID tubes with aluminium inserts at both ends were tested in tension. One reached the Instron interlock at 25.0 kN and failed at the aluminium-adhesive interface at a lower 21.7 kN (17.2 MPa) when re-tested, indicating the first test took the bond close to its maximum failure and began damaging the bond. The second reached 20.6 kN when a testing fixture bolt failed and reached 26.7 kN (21.3 MPa) when re-tested only for a rodend to fail. The testing fixtures and rodends were stepped up in size for the next tests. The third failed at 36.1 kN (28.7 MPa) with an aluminium-adhesive failure. One 16 mm ID tube with one aluminium insert and one titanium insert at each end failed at 26.9 kN (21.4 MPa). With the maximum load case for 16 mm ID links being 7.47 kN in tension, the testing results gave a minimum safety factor of 2.9.

The wishbones are expected to see up to 100,000 cycles over their lifetime, covering 1000 km of driving. With baseline tension testing results obtained, fatigue testing was performed to verify the bond strength over 100,000 cycles of maximum loading, and tension testing until failure was performed after to observe any decrease in bond strength.

One 16 mm ID tube with one aluminium and one titanium insert at each end was subjected to 103,498 fully reversed cycles at 8 kN of loading (Figure 32) without failure. After the fatigue testing, the tube failed at 33.9 kN (27.0 MPa, Figure 33) due to a titanium-adhesive failure. This showed no decrease in bond strength when compared to the baseline testing results, indicating that 8 kN (6.4 MPa) was too low to produce any significant fatigue damage over 100,000 cycles. With a failure safety factor of 4.5, this validated both the aluminium and titanium insert designs.

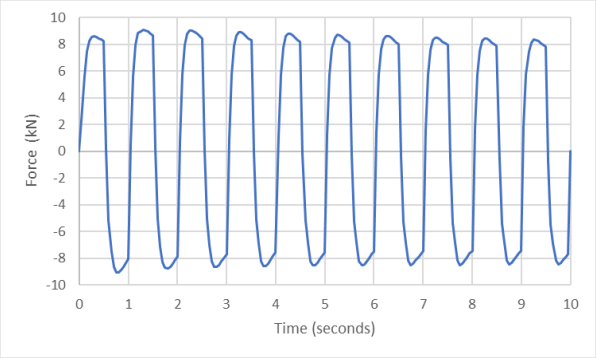

Figure 32 Fatigue testing force input. Force was set to 0 kN setpoint +/- 8 kN amplitude, square shape. Testing occurred for 103,498 cycles.

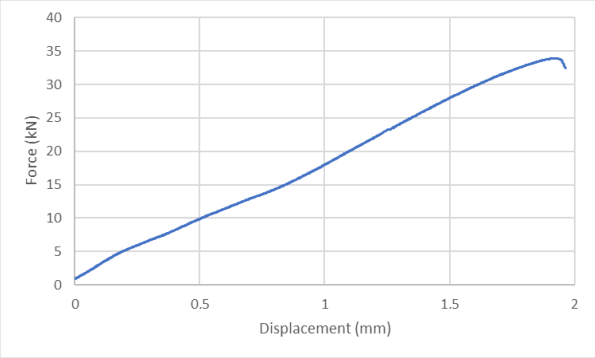

Figure 33 Tension testing after 103,498 fully reversed cycles at 8 kN axial loading. Failure occurred at 33.9 kN. 25 mm inserts, 0.1 mm glue gap, 16 mm ID tube.

One 12 mm ID tube with aluminium inserts at both ends was subjected to 128,753 fully reversed cycles at 4 kN of loading. After the fatigue testing, the tube failed at 24.1 kN (25.6 MPa, 7.0 safety factor, Figure 34) due to a carbon delamination. Again, this showed no decrease in bond strength when compared to the baseline testing results, indicating that 4 kN (4.2 MPa) was too low to produce any significant fatigue damage over 100,000 cycles.

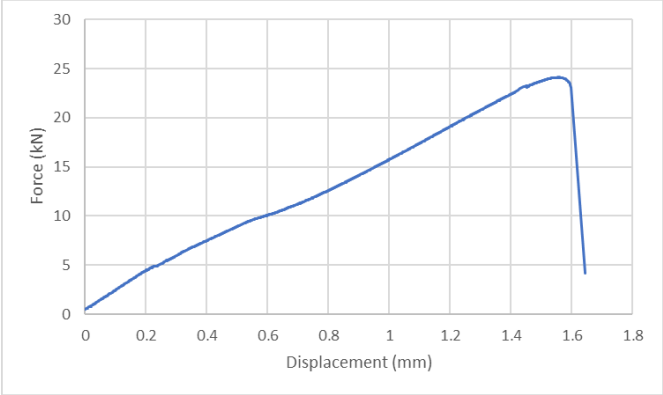

Figure 34 Tension testing after 128,753 fully reversed cycles at 4 kN axial loading. Failure occurred at 24.1 kN. 25 mm inserts, 0.1 mm glue gap, 12 mm ID tube.

Compression testing was also investigated as a potential failure mode. Both a 12 mm ID tube and a 16 mm ID tube were tested in compression up to 30.0 kN without failing. With the inserts not failing in compression, this left buckling a full-length tube as a potential failure mechanism. Euler buckling calculations were performed for every link (Equation 1), each with their own length and maximum compression load case. Johnson buckling was also considered, however every link exceeded the critical slenderness ratio.

$$P_{cr} = \frac{\pi^2 EI}{(KL)^2}$$

Equation 1 Euler buckling: critical force.

The compressive yield strength of the tube was taken as a conservative minimum value calculated from the 12 mm ID tube that reached 30.0 kN of compressive load without failing. The modulus of elasticity was calculated to be 93 GPa based on the flexural stiffness specifications provided by CST Composites. Using this equation, the Front Lower Aft link had the lowest buckling safety factor of 3.4. A representative 390 mm length 16 mm ID tube was tested in buckling (Figure 26). The tube buckled at 32.8 kN (Figure 35), 17% higher than the predicted 28.0 kN. This error is likely due to the assumption of an evenly distributed 93 GPa modulus of elasticity, whereas the different carbon fibre layers and orientations throughout the cross-section will result in an uneven distribution of elasticity. This resulted in a validated safety factor of 3.5 in buckling, and as mechanical testing exceeded predicted results by 17%, buckling was ruled out as a failure mode across all of the links.

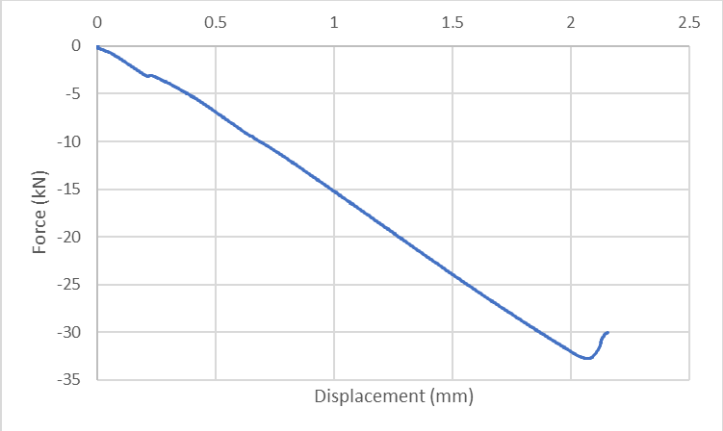

Figure 35 Front lower aft representative buckling test: 390 mm link, pinned ends, 16 mm ID 2mm WT tube, estimated modulus 93 GPa. Aluminium inserts 25 mm length, 0.1 mm glue gap, filament wound tube. Buckling failure occurred at 32.8 kN.

7. ADVANCED ANALYSIS

7.1 Simulation Setup

ANSYS 19.2 Static Structural was used for FEA simulation to measure the stress at the titanium outboards, as well as obtain simulated data for camber and toe compliance.

The model included simplified rodends and spherical bearings, inboard inserts, fore and aft tubes and the titanium outboard (Figure 36).

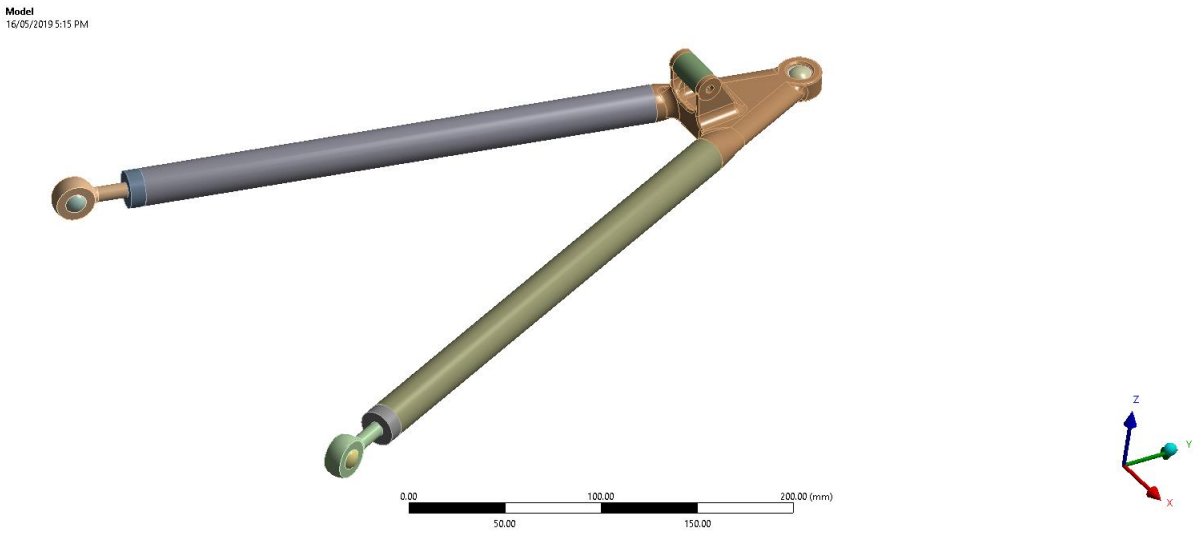

Figure 36 Front right lower CAD model used for wishbone structural analysis with ANSYS Static Structural.

The spherical joints were modelled with frictionless contacts (Figure 76). All other contact areas were bonded contacts (Figure 77).

The outboard spherical bearing was constrained in the z-axis, maintaining a constant height from the contact patch. Rotation in the x-, y- and z-axes was also fixed, this spherical bearing would be clamped onto by mechanical fasteners. It was free to translate in the x- and y- axes (Figure 78).

A spring joint with a preload was used to model the shock bolt clamping force (Figure 79).

The inboard rodend bearings were fixed and the forces were applied through the outboard point and shock point as calculated (Figure 80). The load cases applied to the wishbones are detailed in Tables 2 & 3.

7.2 Simulation Results

The reaction forces at the fore and aft inboard supports were measured to validate the simulated axial forces against the calculated axial forces. Deformation of the outboard point was measured in both the x- and y-axes. The maximum stress in the titanium outboard was measured. The design stress for the titanium was 300 MPa. The design stress considerations for 3D printed titanium are described later in 3D Printing Considerations (Section 8.1). The total deformation of the wishbone was also measured to observe the behaviour of the wishbone under loading. All of the results are detailed in Tables 12-19. The maximum camber compliance of the wishbones was calculated at 0.03 ^{o}/g at the front and 0.04 ^{o}/g at the rear at the maximum pure lateral loadcase.

Table 12 Front lower wishbone simulation results for each load case input.

Load case	Maximum stress (von Mises)	Shock deformation	Outboard x deformation	Outboard y deformation	Fore reaction	Aft reaction
Pure lateral	276 MPa	0.86 mm	-0.04 mm	-0.10 mm	-3006 N	-2116 N
Combined 1	255 MPa	0.98 mm	0.80 mm	-0.05 mm	4922 N	-8044 N
Braking	245 MPa	0.91 mm	0.88 mm	0.05 mm	7693 N	-6523 N
Bump	922 MPa	5.32 mm	0.76 mm	0.12 mm	7316 N	4317 N

Table 13 Rear lower wishbone simulation results for each load case input.

Load case	Maximum stress (von Mises)	Shock deformation	Outboard x deformation	Outboard y deformation	Fore reaction	Aft reaction
Pure lateral	259 MPa	0.66 mm	0.22 mm	-0.12 mm	2029 N	-3819 N
Combined 3	225 MPa	0.72 mm	0.01 mm	-0.03 mm	-849 N	-1459 N
Acceleration	162 MPa	0.69 mm	-0.15 mm	0.07 mm	-2087 N	1643 N
Bump	619 MPa	1.76 mm	0.40 mm	0.01 mm	6742 N	994 N

Table 14 Front upper wishbone simulation results for each load case input.

Load case	Maximum stress	Outboard x deformation	Outboard y deformation	Fore reaction	Aft reaction
Pure lateral	51 MPa	0.03 mm	0.09 mm	1843 N	1419 N
Combined 1	62 MPa	-0.25 mm	0.05 mm	1578 N	3405 N

Table 15 Rear upper wishbone simulation results for each load case input.

Load case	Maximum stress	Outboard x deformation	Outboard y deformation	Fore reaction	Aft reaction
Pure lateral	56 MPa	-0.12 mm	0.11 mm	-534 N	2724 N
Combined 3	50 MPa	-0.13 mm	0.06 mm	-1381 N	1423 N

Table 16 Front toe link simulation results for each load case input.

Load case	Maximum stress	Maximum deformation
Pure lateral	22 MPa	0.01 mm
Combined 1	25 MPa	0.10 mm
Braking	25 MPa	0.10 mm

Table 17 Rear toe link simulation results for each load case input.

Load case	Maximum stress	Maximum deformation
Pure lateral	27 MPa	0.08 mm
Combined 3	42 MPa	0.05 mm
Acceleration	105 MPa	0.14 mm

Table 18 Front camber compliance results.

Load case	Front camber compliance
Pure lateral	0.07^{o}
Combined 1	0.04^{o}

Table 19 Rear camber compliance results.

Load case	Rear camber compliance
Pure lateral	0.08^{o}
Combined 3	0.03^{o}

8. FINAL DESIGN

A mass breakdown is detailed in Table 20. The total mass across the car of the carbon fibre wishbones and links comes to 3137 g, compared to 4854 g for the steel wishbones. This mass saving of 1717 g corresponds to 1.9 points gained at the competition for M19-E and 2.3 points gained for M19-C.

Table 20 Final design mass breakdown by wishbone component.

	FRU	RRU	FRL	RRL	FTL	RTL	Total
Titanium outboard (g)	28	28	107	124			574
Aluminium inserts (g)	20	20	34	34	54	43	410
Carbon tube (g)	80	80	106	67	43	28	805
Total (g)	128	146	265	225	97	71	1789
Steel total (g)	208	204	581	507	130	123	3506
Spherical (g)	18	18	18	18			144
Rodends (g)	42	42	72	72	42	42	624
Fasteners (g)	32	32	42	51	33	33	446
Ferrules (g)	9	9	17	20	6	6	134
Total (g)	101	101	149	161	81	81	1348

Figure 37 Front right carbon fibre wishbones final CAD design and render.

Figure 38 Front lower titanium outboard design, CAD render.

Figure 39 Rear right carbon fibre wishbones final CAD design and render.

Figure 40 Rear lower titanium outboard design, CAD render.

8.1 3D Printing & Post-Machining Considerations

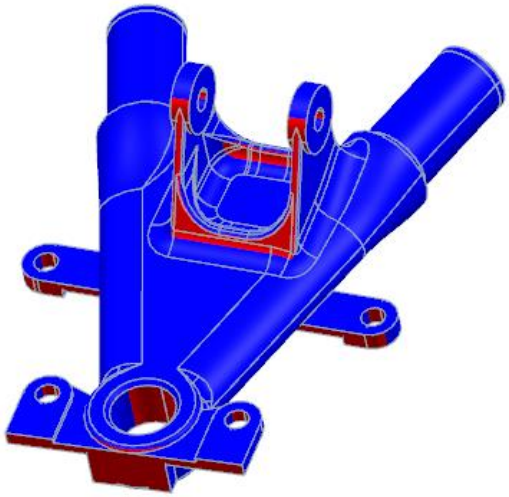

Figure 41 Front right lower titanium outboard. Printing overhang angles greater than 45 degrees (red) require support material.

The printing process can achieve a maximum overhang angle of approximately 45^{o} without requiring support structures. The printing orientation was selected to reduce the need for support structures (Figure 41), specifically along the insert surfaces to provide a high tolerance glue gap with a consistent surface finish to aid adhesive bonding. An extruded square block at the base of the model was recommended to improve the stability of the component during the printing process. This block was added up to where the overhang angle exceeded 45^{o}, and can be removed in the post-machining process.

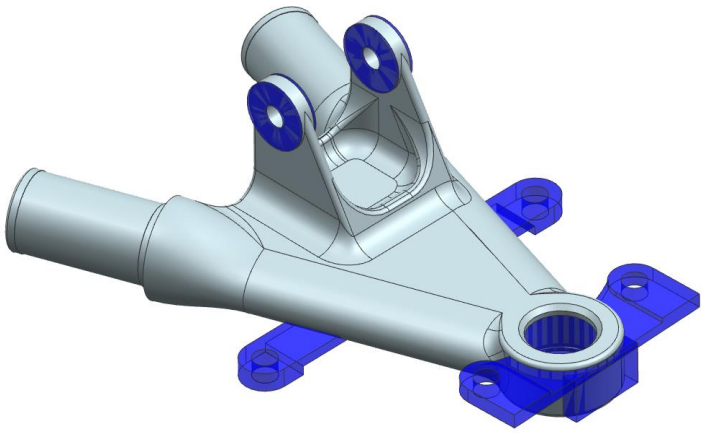

Figure 42 Front lower titanium outboard design. Features to be printed and removed by post-machining processes are highlighted in blue.

The typical surface finish of DMLS Ti-6Al-4V was described as “coarse sandpapery”, with an average particle size of 30 microns (Figure 43). This surface roughness is highly desirable for the adhesive bonding surface by providing an increase in total surface area without any extra coarsening processes, however the bearing cup and clevis surfaces require post-machining for a smooth milled surface finish. An extra 0.5 mm of material was printed on these surfaces to be removed by a CNC

mill operation (Figure 42). Tabs were printed on either side of the bearing cup with a 5 mm hole to be bolted down to a jig for post-machining. A probing operation can be used to find the centre of each bearing cup, so jig precision is not necessary, however jig rigidity is essential to improve the machinability of titanium. For this reason, extra tabs were printed closer to the clevises to improve rigidity for the clevis machining, at the expense of requiring an extra machining setup.

Figure 43 Front upper wishbone inserts and bearing cups printed by MCAM. The rough surface finish can be seen and provides a great adhesive bonding surface.

After printing, the titanium bearing cups underwent hot isostatic pressure (HIP) treatment. HIP treatment is recommended for 3D printed Ti-6Al-4V components designed for fatigue loading. The process involves heating the printed components to 920^{o}C under 100 MPa of isostatic pressure for 120 minutes (Arcam, 2019).

The mechanical properties of Direct Metal Laser Sintered (DMLS) Ti-6Al-4V before and after HIP treatment are shown in Table 21.

Table 21 Material properties of DMLS Ti-6Al-4V, before and after HIP treatment (Mitchell, 2018).

	HIP treated	Non-HIP treated
Yield strength	832 MPa	896 MPa
Ultimate tensile strength	909 MPa	956 MPa
Modulus	112 MPa	118 MPa
Fatigue strength (>10,000,000 cycles)	650 MPa	396 MPa

8.2 Final Assembly Procedure

The final assembly will use the wishbone jigs already manufactured for welding the steel wishbones. The most important step to the process is the surface preparation of the inserts and tube. Aluminium inserts are sandblasted with the coarsest grit available to achieve a consistently rough surface finish. The inside of the carbon tubes is sanded with 40 grit sandpaper until the inner layer of glossy epoxy is removed. These surfaces are blown dry with compressed air to remove abrasive debris, soaked in an acetone bath for five minutes, and then blown dry again with compressed air. Adhesive should be applied to both surfaces, be generous. The carbon tube should be masked with tape to prevent any adhesive curing on the surface. The inboard aluminium inserts are glued first,

and when dry can be drilled and tapped to ensure concentricity. The titanium outboard inserts are to be glued on the wishbone jigs to achieve an accurate wishbone geometry.

9. CONCLUSIONS

Carbon fibre wheel shells were designed with a minimum safety factor of 1.14. The total mass came to 4280 g, saving 3760 g compared to the aluminium wheel shells. This corresponds to 3.0 points gained at the competition for M19-E and 3.8 points gained for M19-C. The number of carbon fibre plies varies from 10 to 16 plies. The layup shapes, orientation and sequence is detailed in Tables 22-25. The simulated camber compliance is 0.16 ^{o}/g for the front and 0.20 ^{o}/g. The carbon fibre wishbones and links design came to 3137 g, saving 1717 g compared to the steel wishbones. This corresponds to 1.9 points gained at the competition for M19-E and 2.3 points gained for M19-C. The wishbone links and adhesive bonding techniques used in the design and manufacture were mechanically validated in tension, compression, fatigue and buckling. The simulated camber compliance is 0.03 ^{o}/g at the front and 0.04 ^{o}/g at the rear. Lab 22 and MCAM have provided Monash Motorsport with titanium 3D printing services to make these designs possible.

10. ACKNOWLEDGEMENTS

Firstly, thanks to the entire Monash Motorsport team, I learnt so much from so many people along the way to make this report possible. Thanks to Scott Wordley for supervising the project and supporting the team for so many years. I'm extremely grateful for the 3D printing services sponsored by Lab 22 and MCAM, which allowed the wishbone design to become possible. Lastly, thanks to Leon Shi for performing the Instron testing.

11. REFERENCES

ARCAM, AB. (2019, January 28). *Arcam EBM System.* Retrieved from Arcam Web Site: http://www.arcam.com/wp-content/uploads/Arcam-Ti6Al4V-Titanium-Alloy.pdf

ANSYS. (2017). *Guide to Composite Failure Criteria*. Retrieved from ANSYS Composite PrepPost User's Guide: https://www.sharcnet.ca/Software/Ansys/17.2/en-us/help/acp_ug/acp_compmodel_compfailure.html

Element Custom Wheels and Tires. (2019, May 14). *Custom Wheels Offset - Guide to Measuring and Understanding Backspacing*. Retrieved from Element Custom Wheels and Tires: https://www.elementwheels.com/custom-wheels-offset

Germany, F. S. (2018). *Disciplines*. Retrieved from Formula Student Germany: International Design Competition: https://www.formulastudent.de/about/disciplines/

Kaw, A. (2006). *Mechanics of Composite Materials.* Boca Raton: Taylor & Francis Group.

Leung, E. (2007). Design and Manufacture of Formula SAE Wheels. *RMIT University Final Year Project*.

McRedie, H. (2015). Determination of the Material Properties of Pre-Impregnated Carbon Fibre. *Monash University Final Year Project*.

Mitchell, B. (2018). The Effect of HIP Treatment on Direct Metal Laser Sintered Titanium Alloy (Ti6Al4V). *Orthopaedic Proceedings*.

Scott, M. (2014). Carbon Wheel Shells for a Formula SAE Vehicle. *Monash University Final Year Project*.

12. APPENDICES

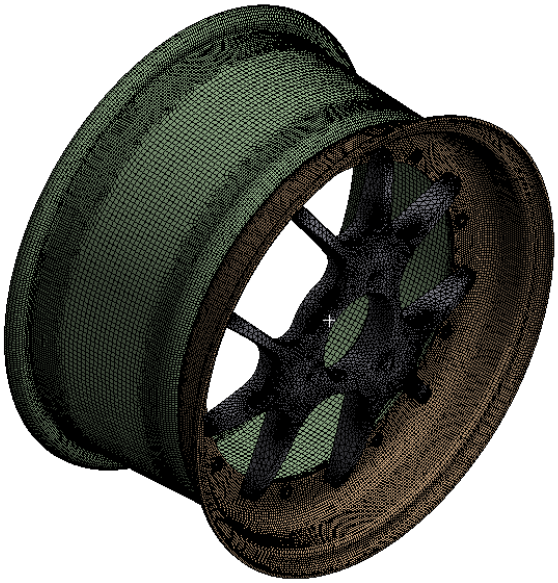

Figure 44 ANSYS front wheel mesh used for advanced analysis.

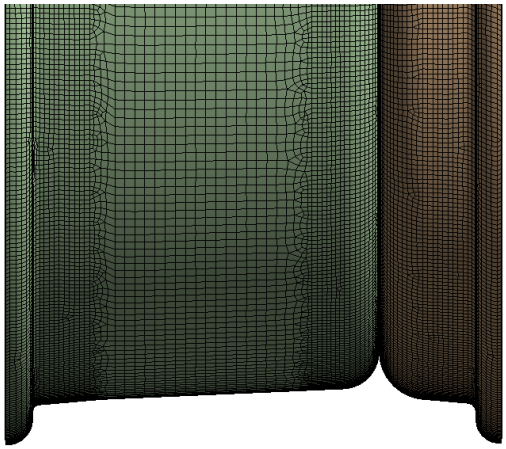

Figure 45 ANSYS front wheel shell mesh, with an element size of 2 mm around the wheel shell bead and flange surfaces.

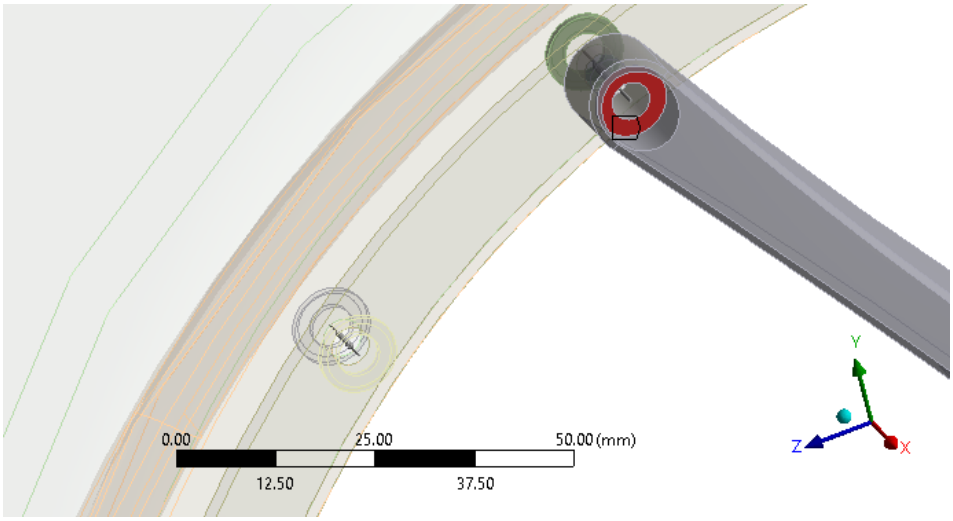

Figure 46 Longitudinal spring joint used to model the bolt clamping force between the wheel centre and inner wheel shell.

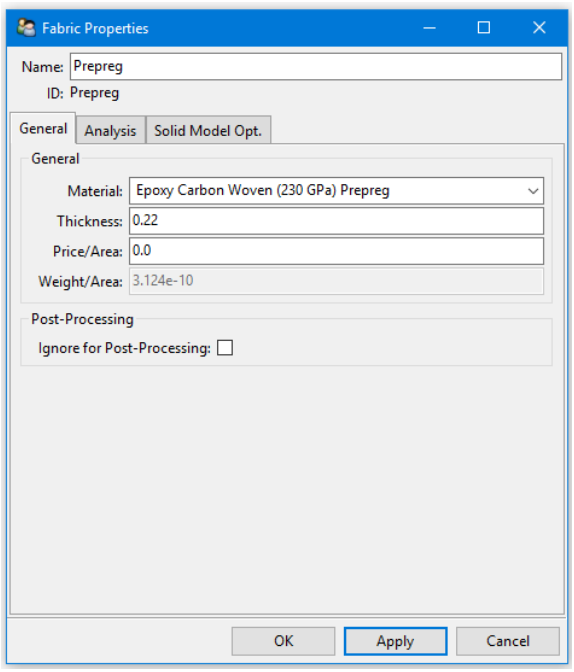

Figure 47 Fabric properties: 0.22 ply thickness is applied to the prepreg material.

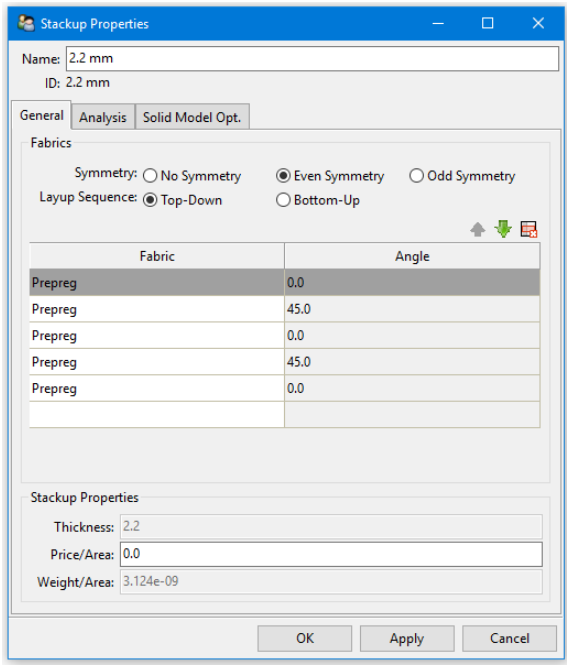

Figure 48 Stackup properties: a 10 ply fabric with alternative 0 and 45 degree fabric orientations. The stackup sequence is even symmetric, applied from the top face down.

Figure 49 An edgewise rosette following the profile of the wheel shell around its full revolution. Direction 1 and 2 define the material 0 and 90 degree orientations.

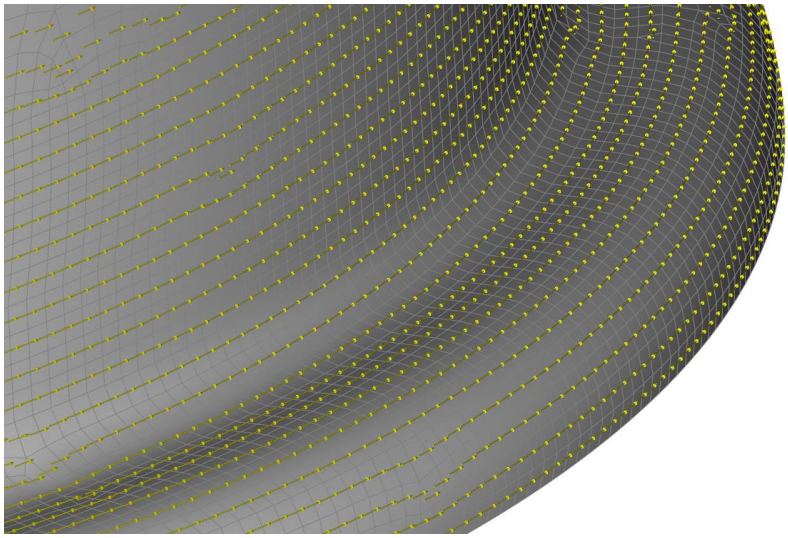

Figure 50 Reference 0 degree orientation around the wheel shell beading surface after applying the rosette reference coordinate system to the wheel shell face.

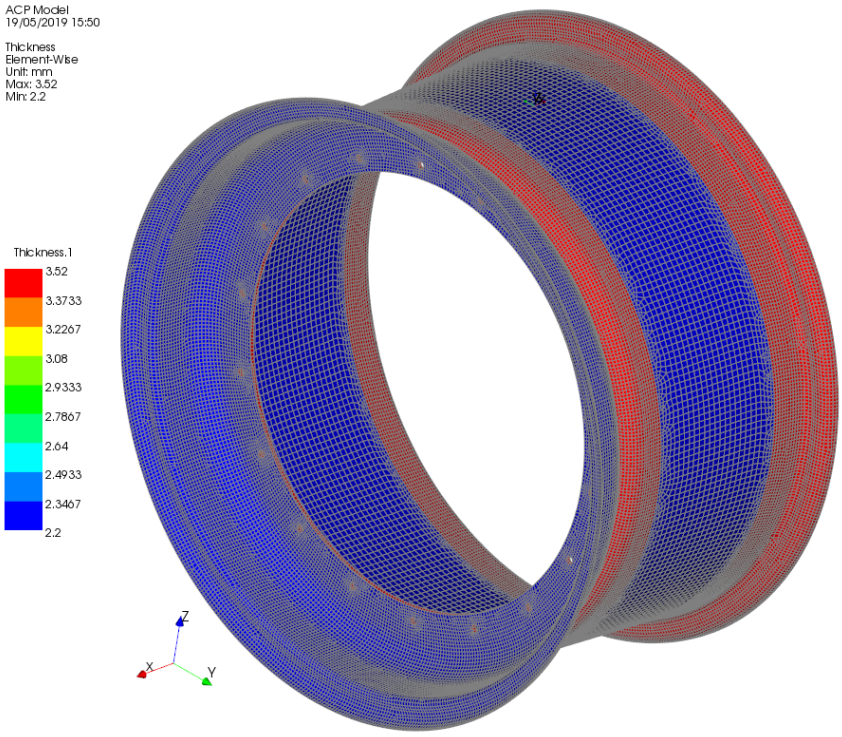

Figure 51 Different thicknesses at each wheel shell segment by applying different carbon fibre stack-ups to the faces.

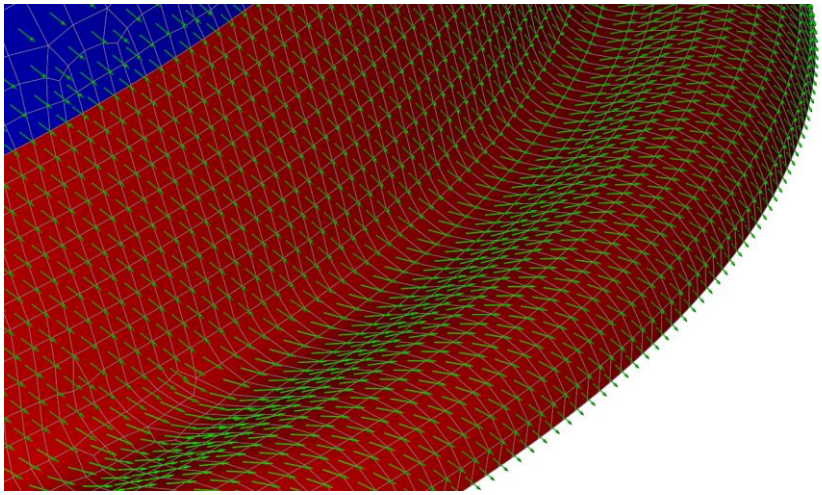

Figure 52 The material direction at each node on the wheel shell of a 45 degree oriented ply.

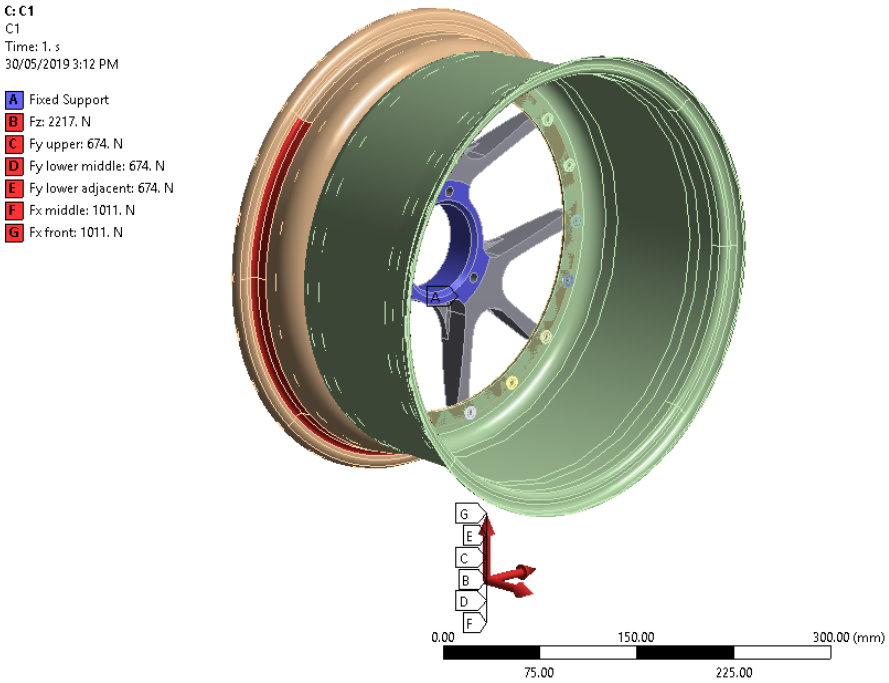

Figure 53 Contact patch forces and wheel centre fixed support used for simulation, inside view.

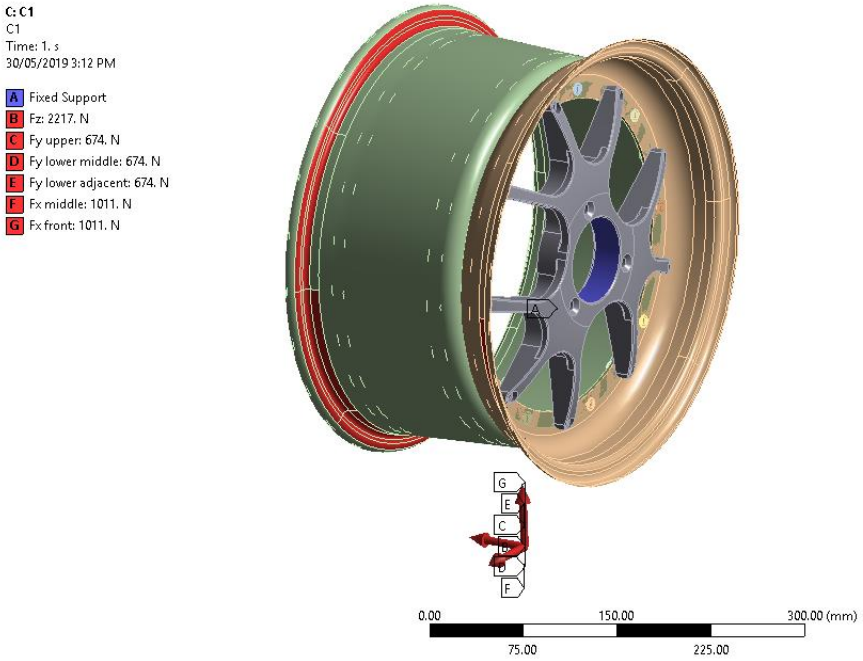

Figure 54 Contact patch forces and wheel centre fixed support used for simulation, outside view.

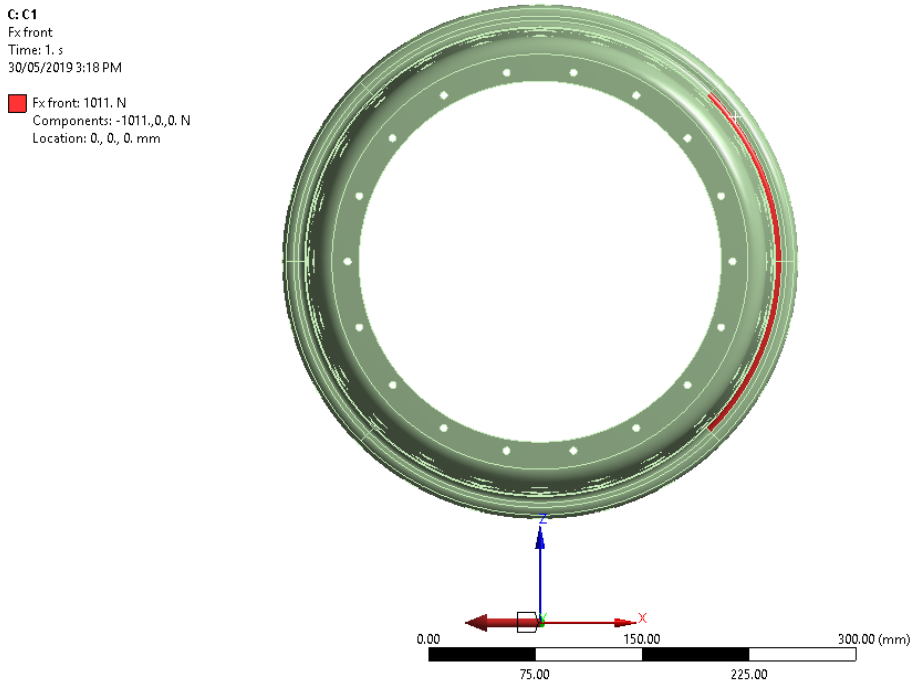

Figure 55 50% of the Fx contact patch force is applied to the front of the rim, evenly distributed between the inner and outer shells.

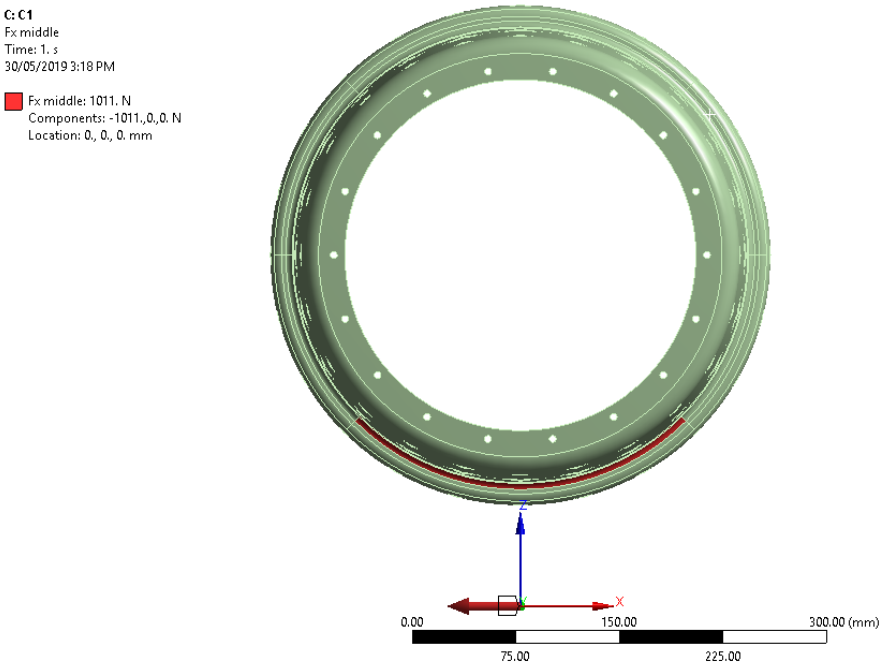

Figure 56 50% of the Fx contact patch force is applied to the bottom of the rim, evenly distributed between the inner and outer shells.

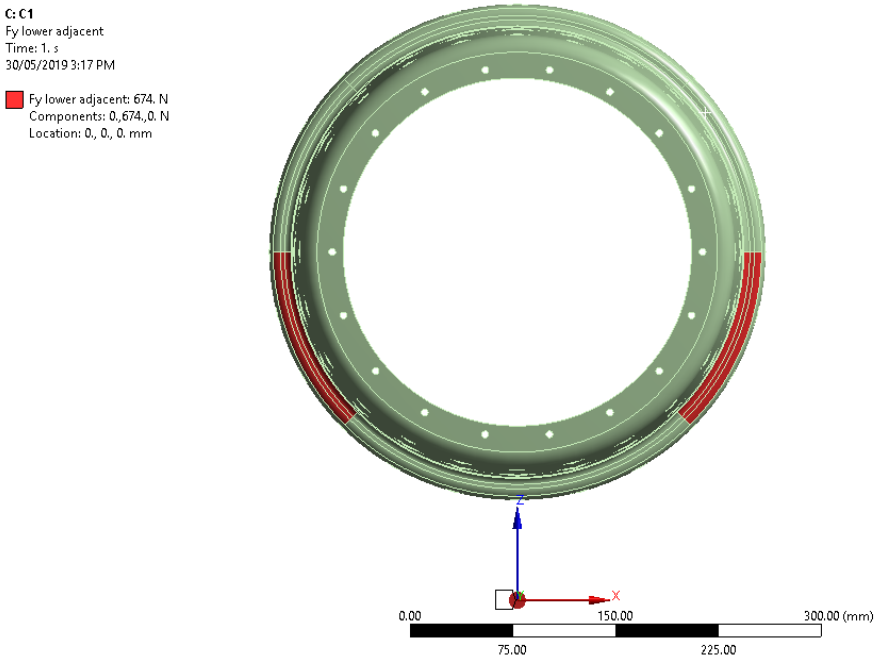

Figure 57 33% of the Fy contact patch force is applied to the lower sides of the inner shell.

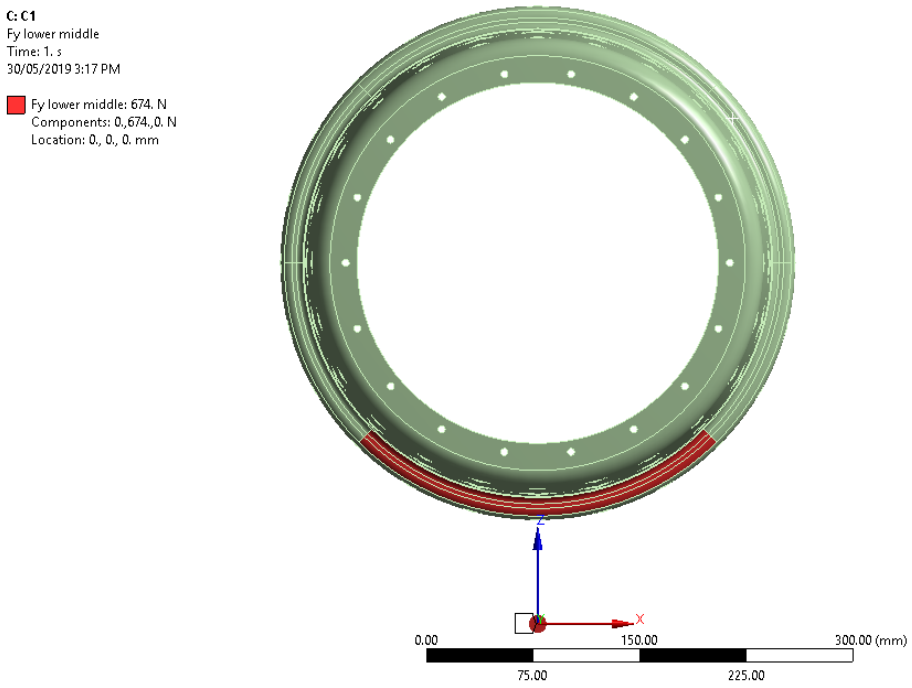

Figure 58 33% of the Fy contact patch force is applied to the lower middle of the inner shell.

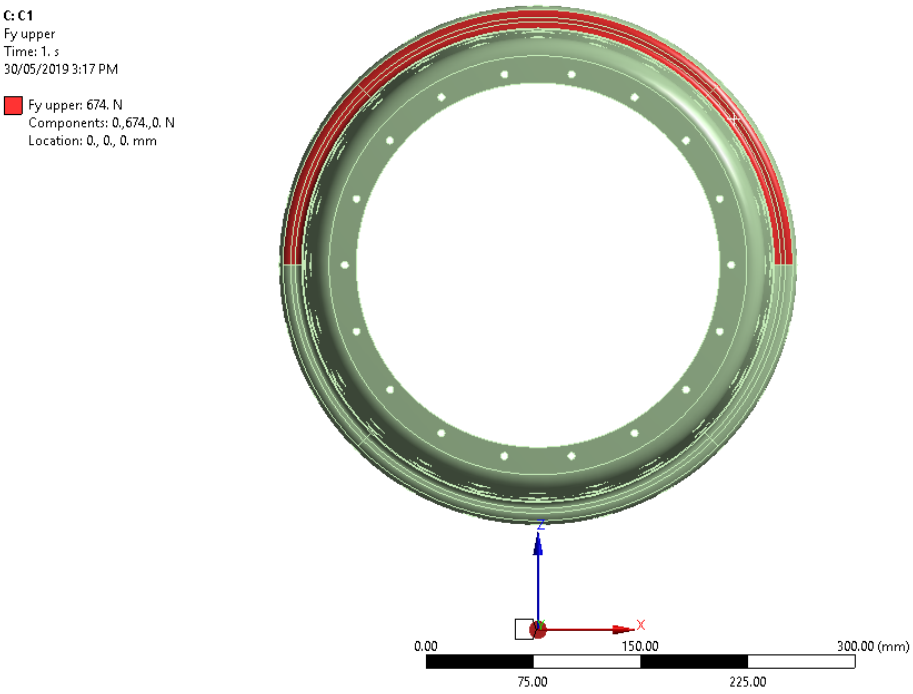

Figure 59 33% of the Fy contact patch force is applied to the top of the inner shell.

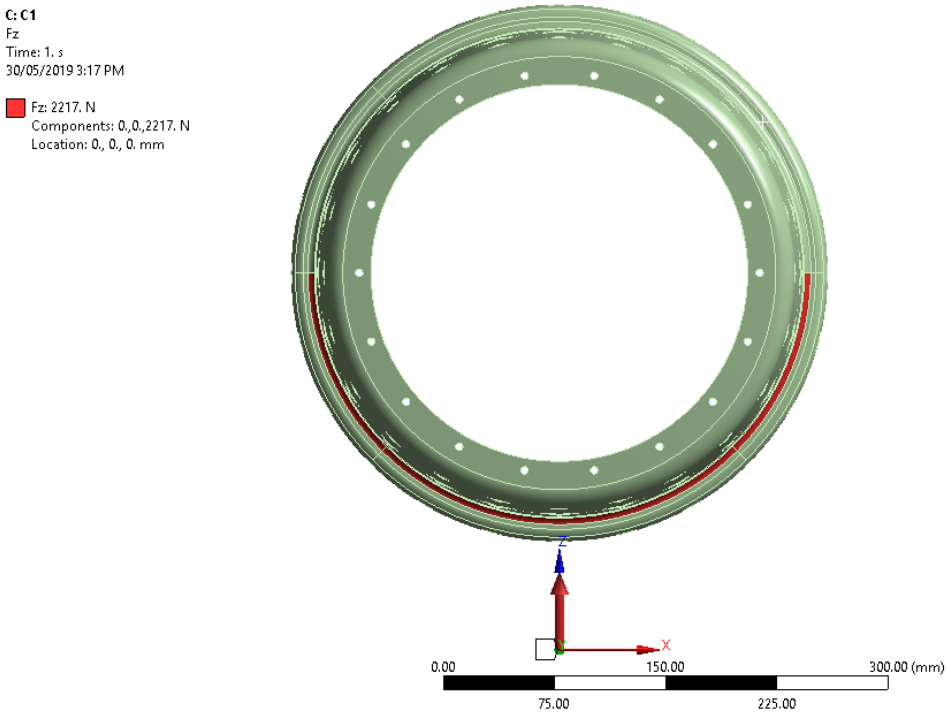

Figure 60 The Fz contact patch force is applied to the bottom of the rim, evenly distributed between the inner and outer shells.

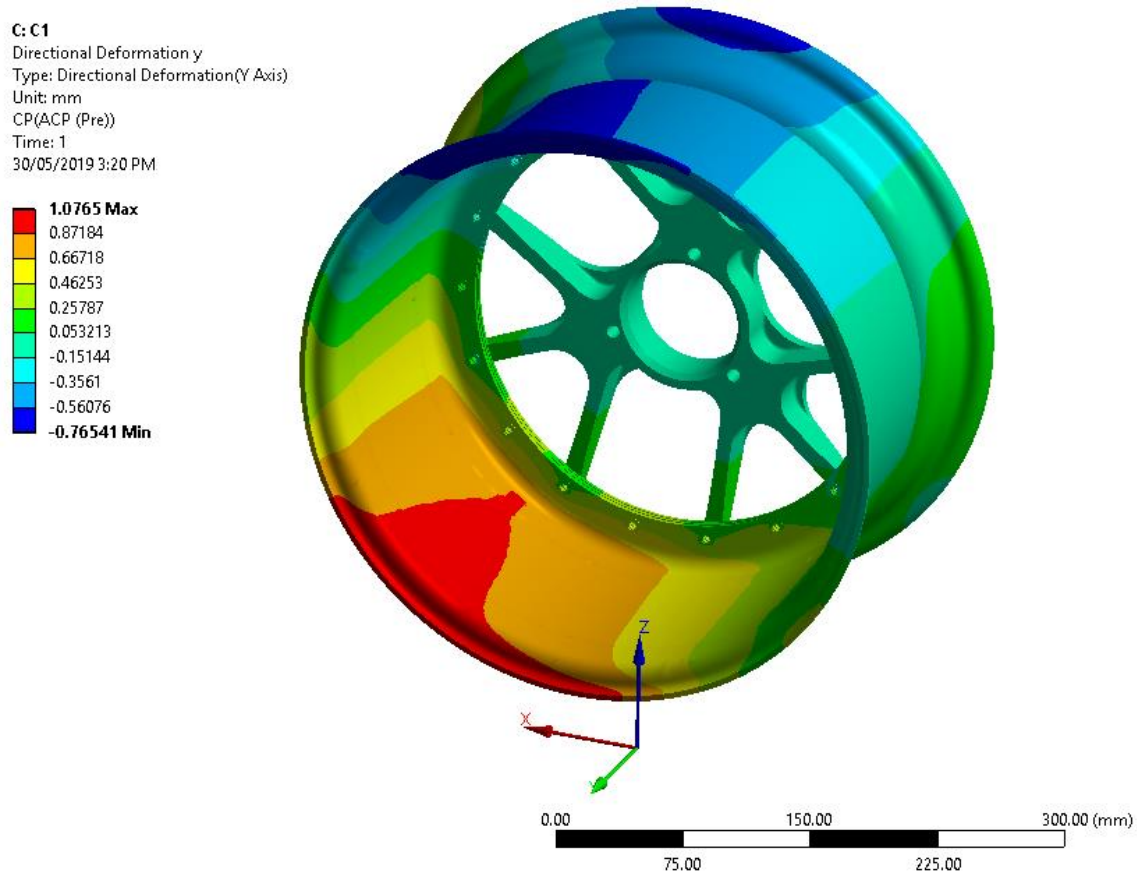

Figure 61 Y-axis directional deformational results, front combined 1 loadcase.

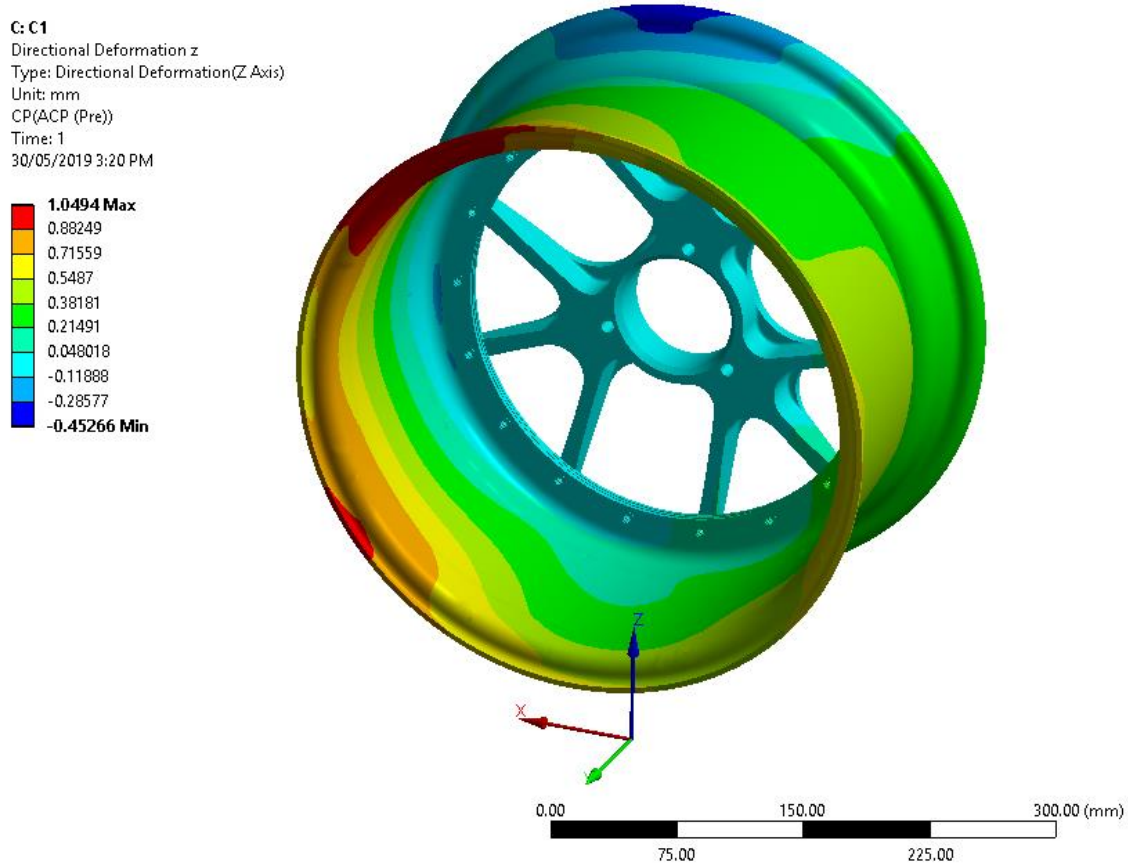

Figure 62 Z-axis directional deformational results, front combined 1 loadcase.

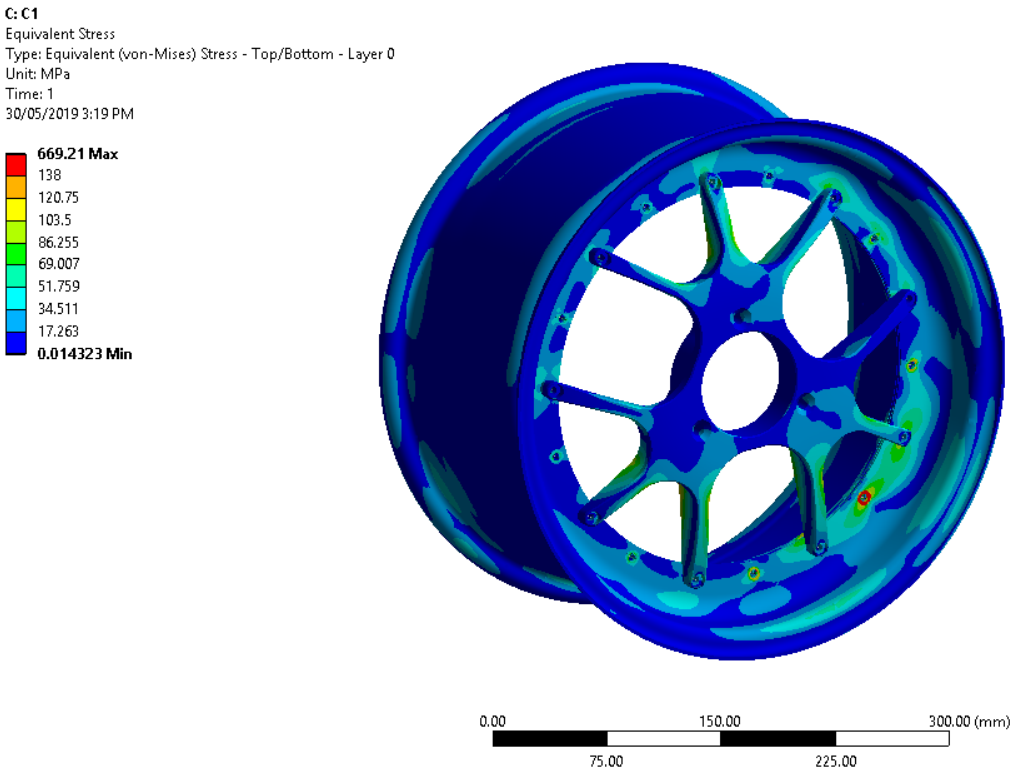

Figure 63 Equivalent von-Mises stress results, front combined 1 loadcase.

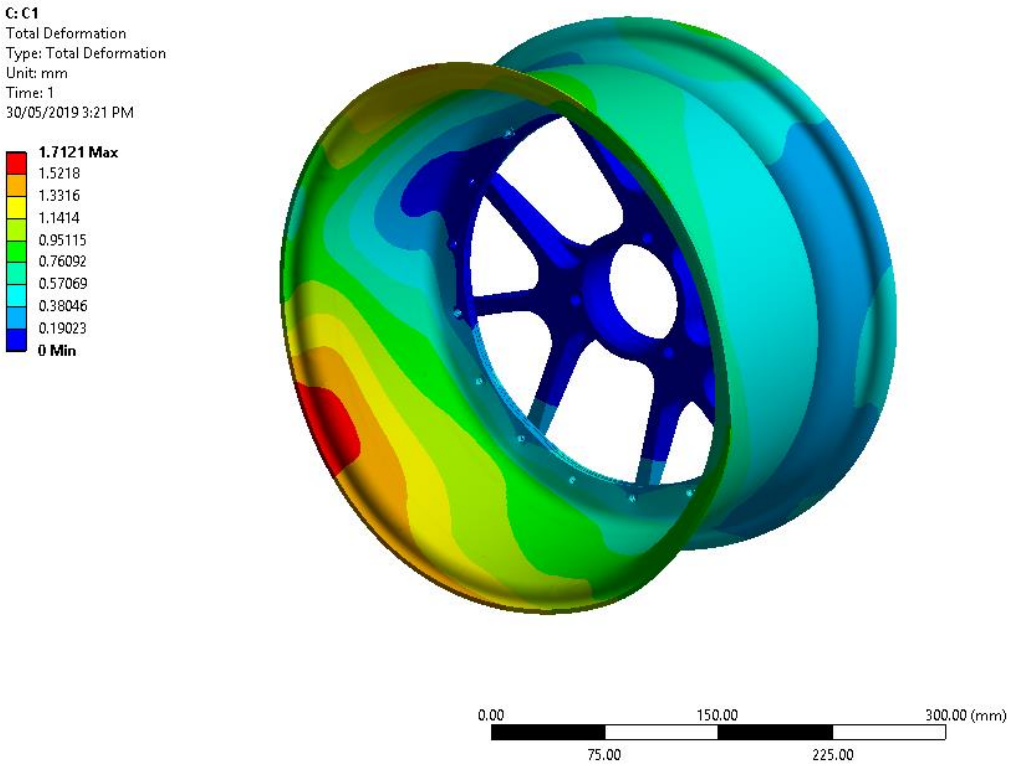

Figure 64 Total deformation results, front combined 1 loadcase.

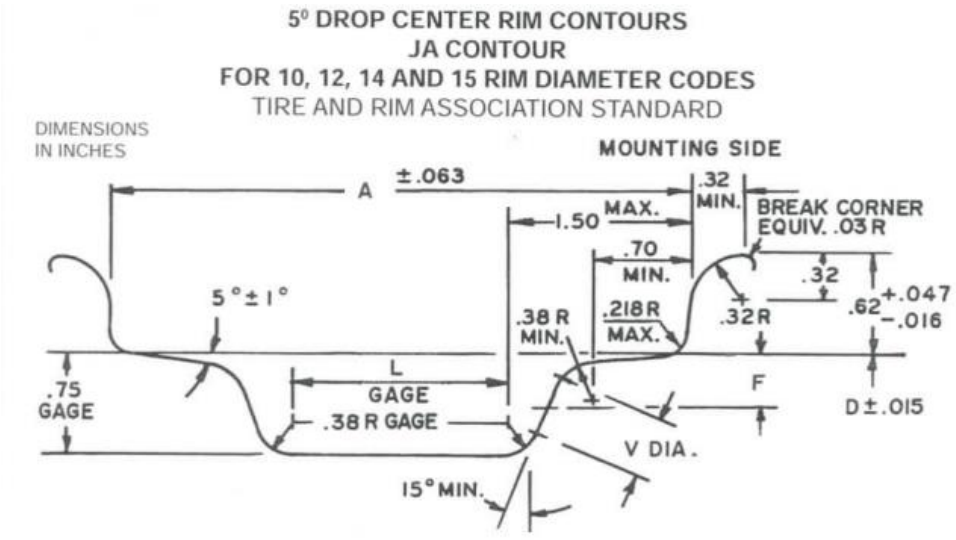

RIM CONTOUR	A	L GAGE
4 JA	4.00	.90
4 1/2 JA	4.50	1.40
5 JA	5.00	1.90
6 JA	6.00	2.90
7 JA	7.00	3.90
8 1/2 JA	8.50	5.41
9 1/2 JA	9.50	6.41
10 1/2 JA	10.50	7.41

RIM DIAMETER CODE	D	V	F
10	9.968	.445/.461	.44 ± .03
12	11.968	.445/.461	.44 ± .03
14	13.968	.445/.461	.44 ± .03
15	14.968	.618/.633	.56 ± .03

Figure 65 Tyre and Rim Association RJ contour used for the design of the wheel shells.

Table 22 Shapes and sequences of the rear inner wheel shell layup.

Rear inner		
Shape	Direction	Quantity
Donut	0	1
Tophat	0	1
Wrap	0	1
45	45 right	6 spaced 60°
Donut	30	1
Tophat	30	1
0-90	0	6 spaced 60°
45	45 left	6 spaced 60°
Donut	60	1
Tophat	60	1
0-90	0	6 spaced 60°
0-90	0	6 spaced 60°
Tophat	60	1
Donut	60	1
45	45 left	6 spaced 60°
0-90	0	6 spaced 60°
Tophat	30	1
Donut	30	1
45	45 right	6 spaced 60°
Wrap	0	1
Tophat	0	1
Donut	0	1

Table 23 Shapes and sequences of the rear outer wheel shell layup.

Rear outer		
Shape	Direction	Quantity
Donut	0	1
Tophat	0	1
Wrap	0	1
45	45 right	6 spaced 60°
0-90	0	6 spaced 60°
Donut	45	1
Tophat	45	1
45	45 left	6 spaced 60°
0-90	0	6 spaced 60°
0-90	0	6 spaced 60°
45	45 left	6 spaced 60°
Tophat	45	1
Donut	45	1
0-90	0	6 spaced 60°
45	45 right	6 spaced 60°
Wrap	0	1
Tophat	0	1
Donut	0	1

Table 24 Shapes and sequences of the front inner wheel shell layup.

Front inner		
Shape	Direction	Quantity
Donut	0	1
Tophat	0	1
Wrap	0	1
45	45 right	6 spaced 60°
Donut	30	1
Tophat	30	1
0-90	0	6 spaced 60°
Donut	60	1
Tophat	60	1
45	45 left	6 spaced 60°
Donut	0	1
Tophat	0	1
0-90	0	6 spaced 60°
0-90	0	6 spaced 60°
Tophat	0	1
Donut	0	1
45	45 left	6 spaced 60°
Tophat	60	1
Donut	60	1
0-90	0	6 spaced 60°
Tophat	30	1
Donut	30	1
45	45 right	6 spaced 60°
Wrap	0	1
Tophat	0	1
Donut	0	1

Table 25 Shapes and sequences of the front outer wheel shell layup.

Front outer		
Shape	Direction	Quantity
Tophat	0	1
Tophat	30	1
Tophat	60	1
Tophat	0	1
Tophat	30	1
Tophat	60	1
Tophat	0	1
Tophat	30	1
Tophat	60	1
Tophat	0	1

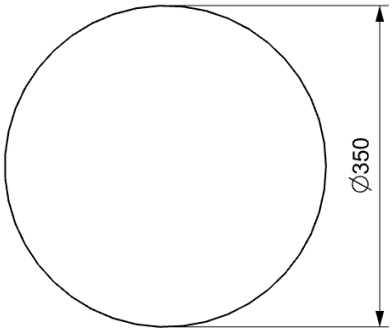

Figure 66 "Tophat" carbon fibre cutout for the front inner and rear wheel shells.

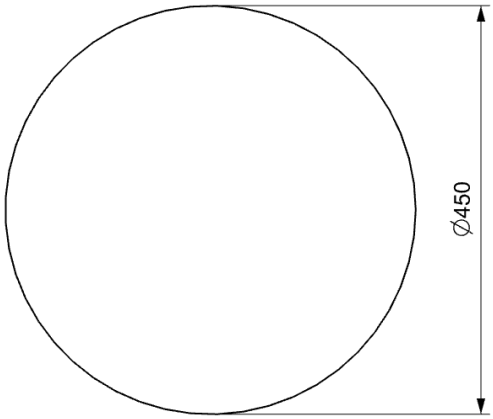

Figure 67 "Tophat" carbon fibre cutout for the front outer wheel shells.

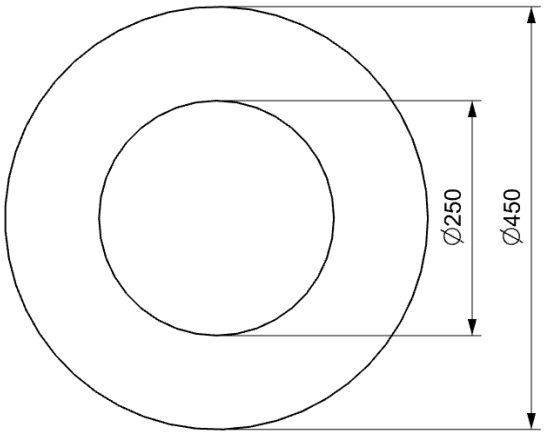

Figure 68 "Tophat" carbon fibre cutout for the front inner and rear wheel shells.

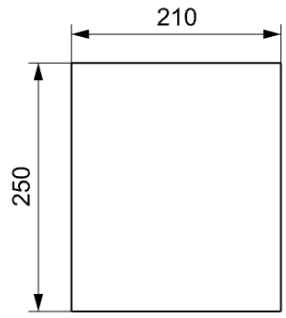

Figure 69 "0-90" carbon fibre cutout for the front inner and rear wheel shells.

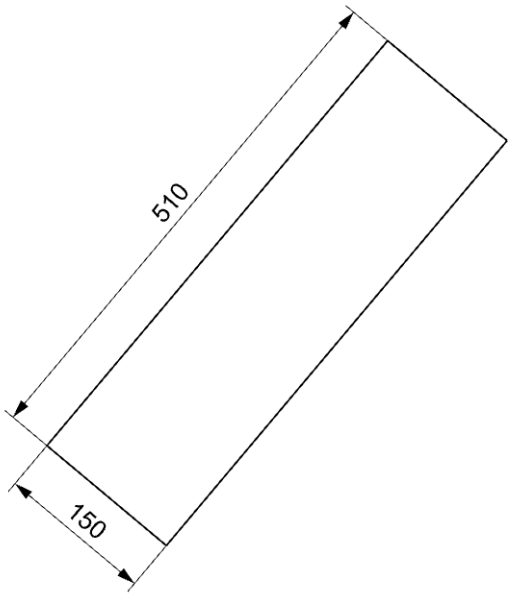

Figure 70 "45 (right)" carbon fibre cutout for the front inner and rear wheel shells.

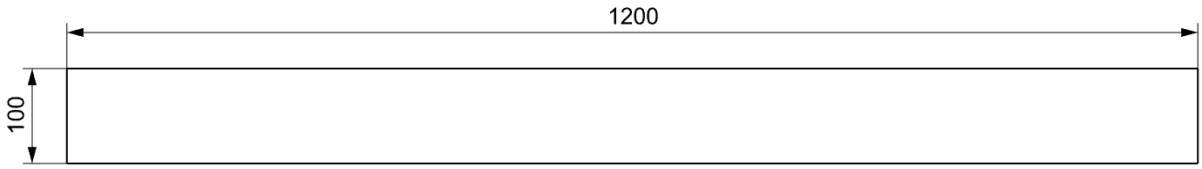

Figure 71 "Wrap" carbon fibre cutout for the front inner wheel shells.

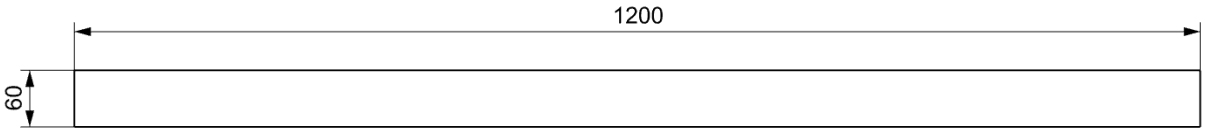

Figure 72 "Wrap" carbon fibre cutout for the rear wheel shells.

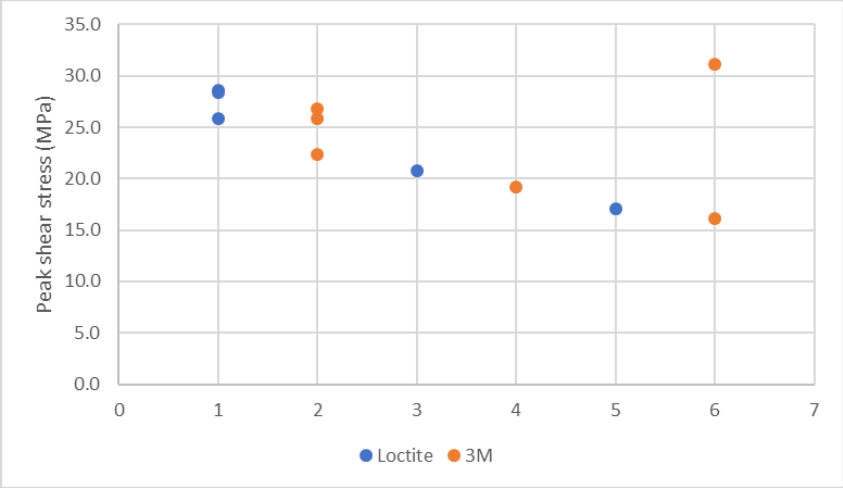

Figure 73 Additional tension testing results normalised for adhesive surface area: all aluminium inserts 15 mm in length, 0.2 mm glue gap. 1-2: 10 mm ID pultruded tube. 3-4: 10 mm ID roll wrapped tube. 5-6: 18 mm ID roll wrapped tube.

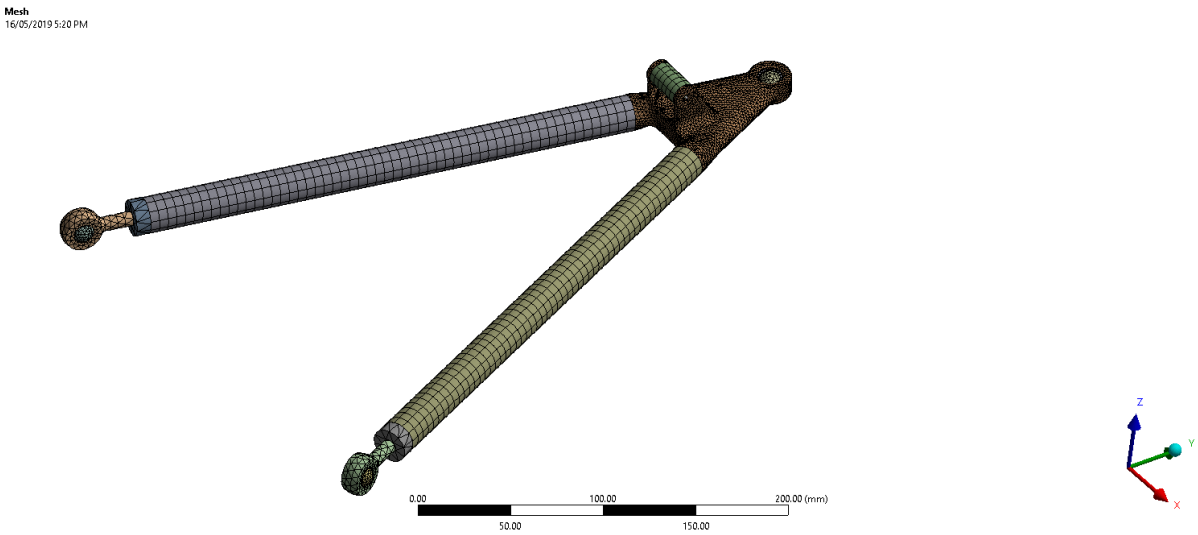

Figure 74 ANSYS front lower wishbone used for advanced analysis.

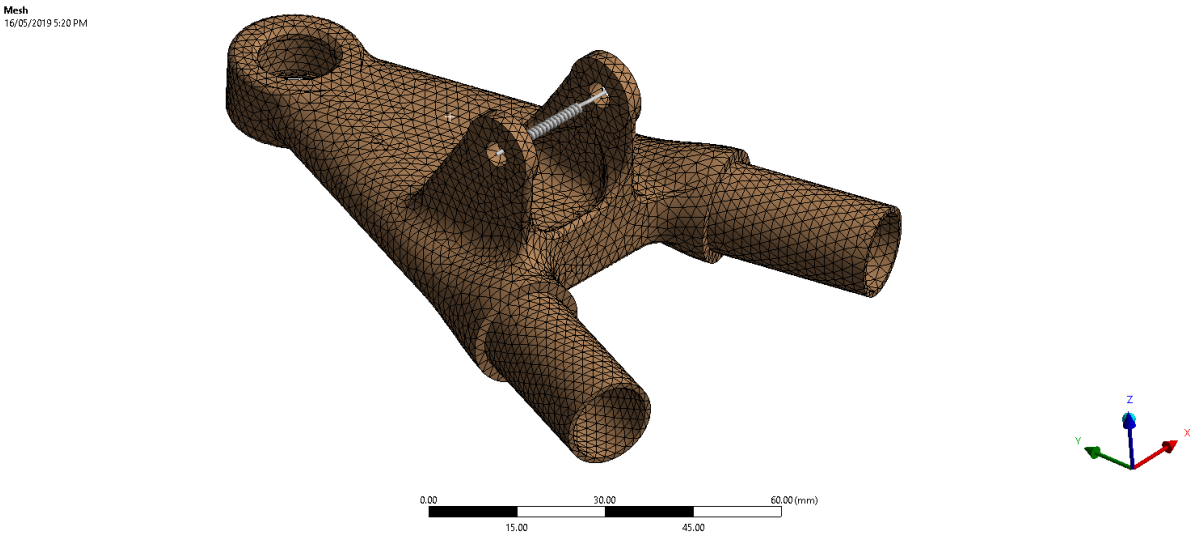

Figure 75 ANSYS front lower titanium outboard mesh with an element size of 2 mm.

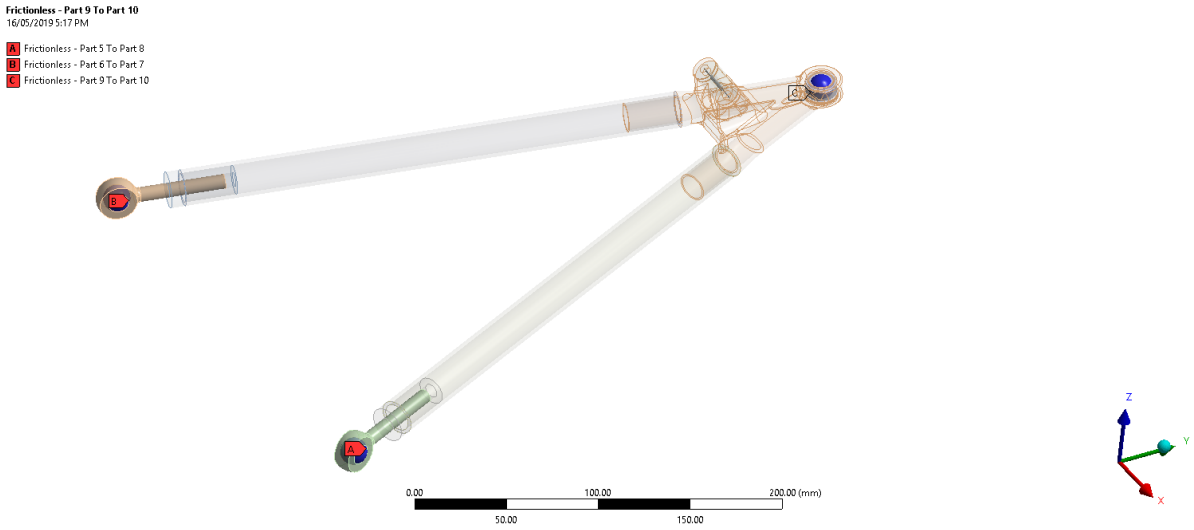

Figure 76 Frictionless contacts used to model the wishbone bearings in ANSYS.

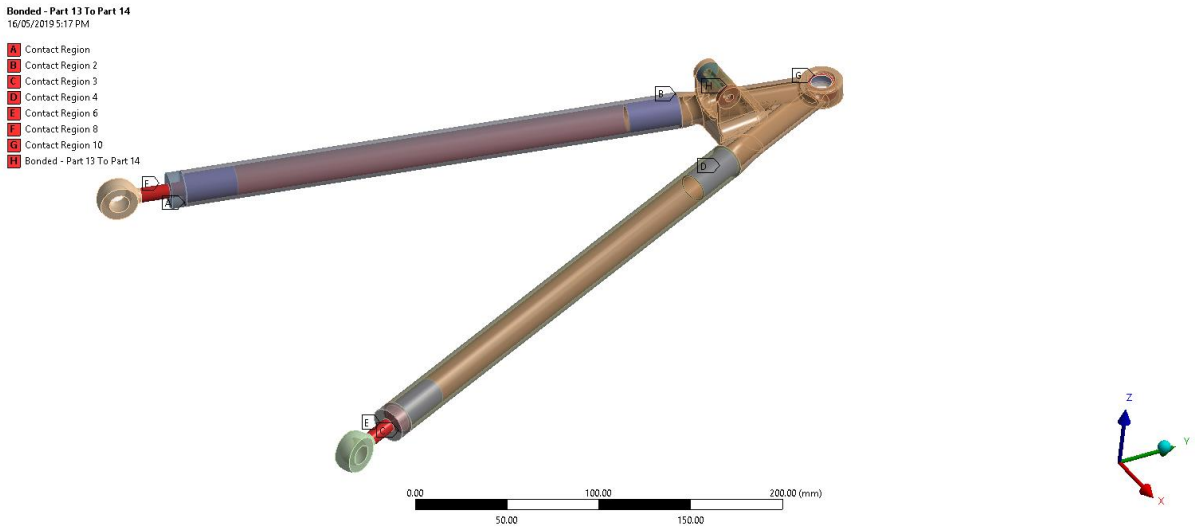

Figure 77 Bonded contacts between bonded components used in ANSYS.

Figure 78 Fixed z-axis translation and fixed rotation at the outboard spherical bearing.

Figure 79 Longitudinal spring joint used to model the bolt clamping force of the shock clevis.

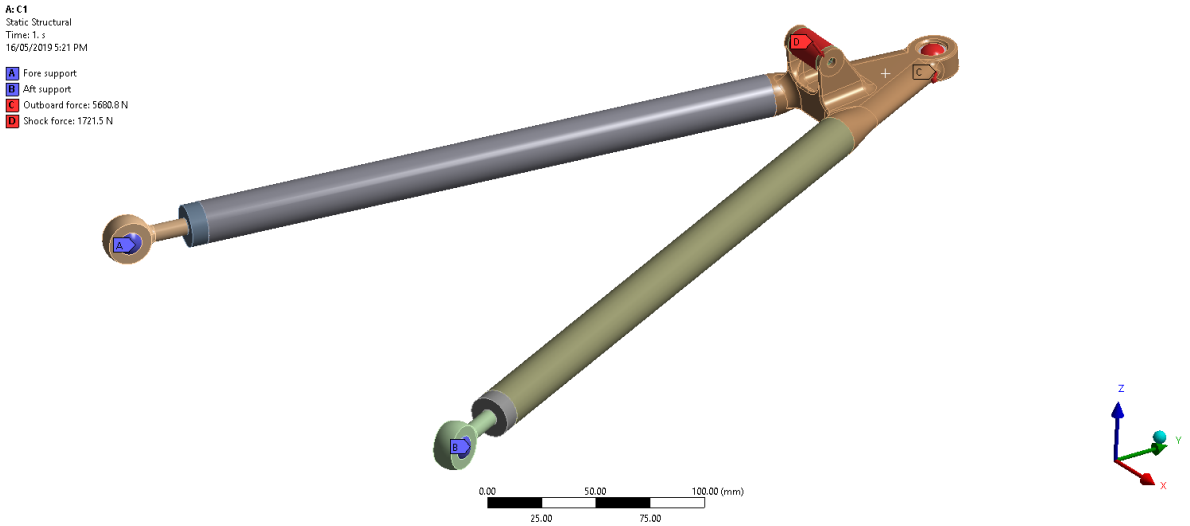

Figure 80 Fixed supports at the inboard rodends. Forces applied at the outboard spherical and shock clevis, combined 1 load case.

Figure 81 Front lower fore reaction force, combined 1 load case.

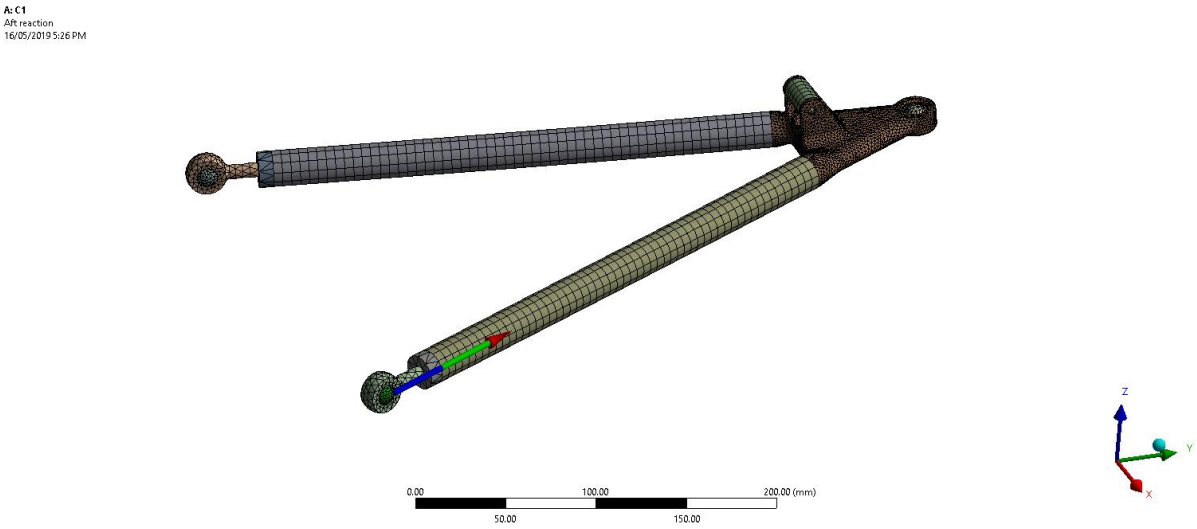

Figure 82 Front lower aft reaction force, combined 1 load case.

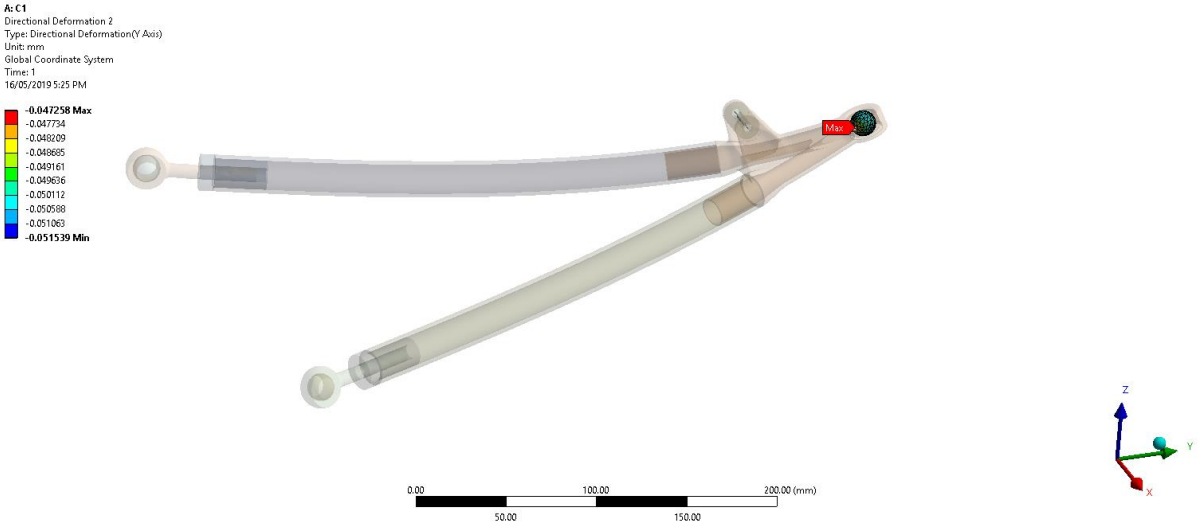

Figure 83 Front lower fore y-axis directional deformation simulation results, combined 1 load case.

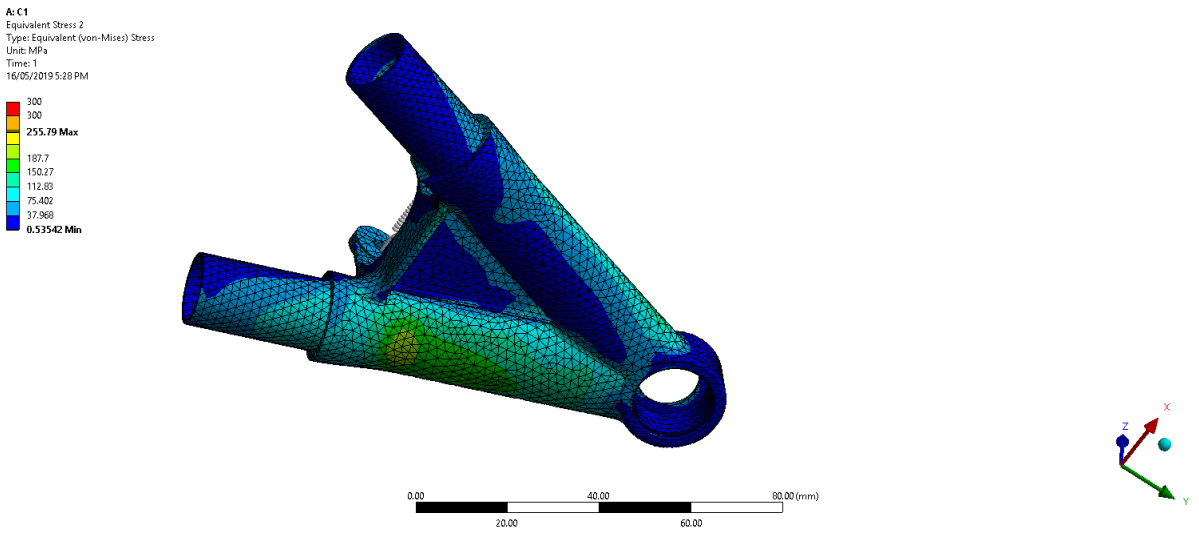

Figure 84 Front lower fore titanium outboard equivalent von-Mises stress simulation results, combined 1 load case, bottom view.

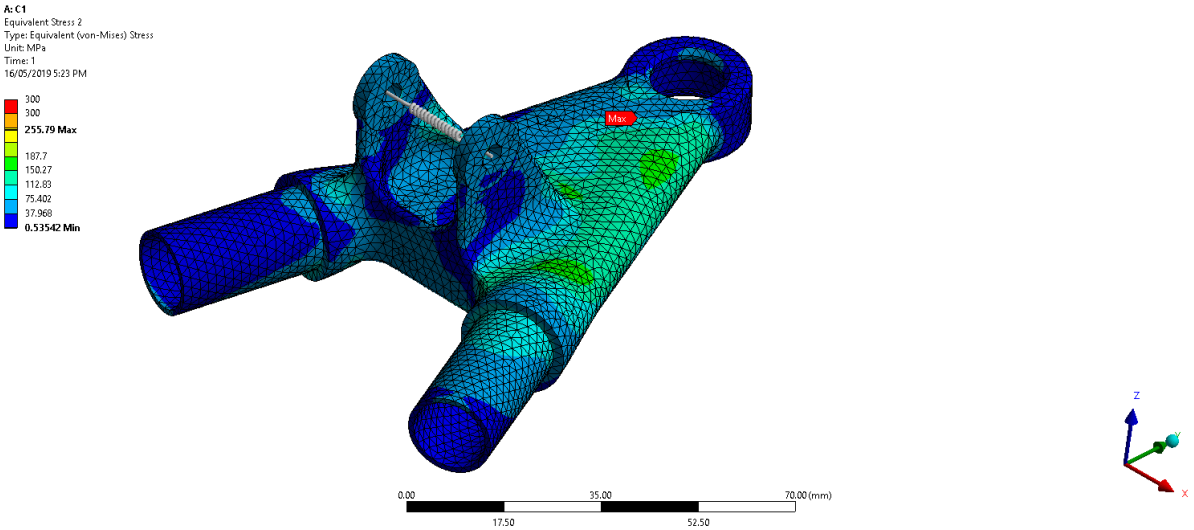

Figure 85 Front lower fore titanium outboard equivalent von-Mises stress simulation results, combined 1 load case, top view.

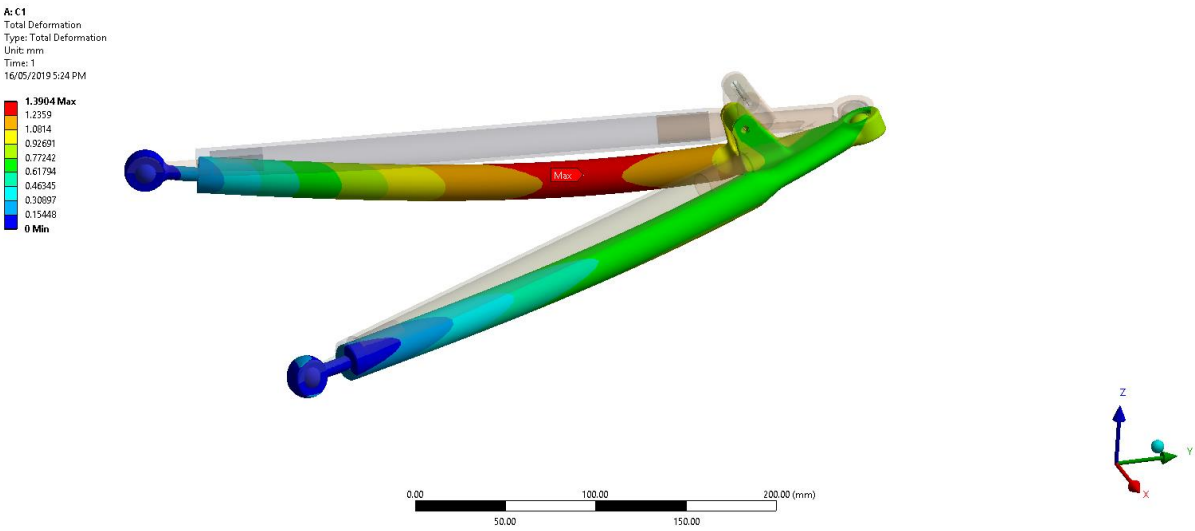

Figure 86 Front lower fore total deformation simulation results, combined 1 load case.